

VOL. 1

NO.1

GEOTECHNICAL JOURNAL



JUNE 1990

SRI LANKAN GEOTECHNICAL SOCIETY

Published by: Sri Lankan Geotechnical Society

EDITORS (SLGS Journal)

J.J.P.Amaratunghe
N.Loganathan

EDITORIAL ADVISERS

A.Thurairajah (Sri Lanka)	A.S.Balasubramaniam (Thailand)
R.K.Bandari (India)	S.M.A.Perera (Sri Lanka)
K.Arulanandam (USA)	T.Sivapatham (Sri Lanka)
H.N.Seneviratna (Sri Lanka)	A.Anandarajah (USA)
E.W.Brand (Hong Kong)	

SLGS Executive Committee

A.Thurairajah	President
K.S.Senanayake	Vice President
T.Sivapatham	Secretary
M.P.J.Jayawardhana	Treasurer
H.N.Seneviratne	Member
D.P.Mallawarachchi	Member
D.W.R.Weerakoon	Member
B.L.Tennekoon	Member
E.J.S.Perera	Member
T.Sritharan	Editor(SLGS News)

Geotechnical Journal is the official publication of the Sri Lankan Geotechnical Society. It is published bi-annually in June and December. Papers are invited for publication in the Geotechnical Journal. Details can be obtained from:

The Secretary, SLGS
c/o National Building Research Organisation,
99/1, Jawatta Road,
Colombo-05,
Sri Lanka.

Telephone 501834, 588946

GEOTECHNICAL JOURNAL

VOLUME 01 NUMBER 01 JUNE 1990

CONTENTS

Evaluation of Slope Stability Analyses C.F.Leung, G.P.Karunaratne and W.G.Quah	1
The Selection of the most appropriate model for 1-D Consolidation B.L.Tennekoon	17
Design Aspects of the Deep Grout Curtain -Randenigala Dam A.U.Gunasekera	34
Undrained Behavior of K_0 Consolidated Clays at Failure S.Thevanayagam	62

NOTE:

Discussions may be submitted on any paper published in this Journal. Discussion of a paper is open to anyone who has significant comments or questions regarding the content of the paper. Discussions are accepted for a period of 3 months following the date of publication of a paper.

EVALUATION OF SLOPE STABILITY ANALYSES

By Leung C.F.¹, Karunaratne G.P.² and Quah W.G.³

ABSTRACT: Many methods developed for slope stability analysis were based on the method of slices and limit equilibrium analysis. In this paper the factors of safety obtained from a number of methods are compared based on a few case studies of test embankments built to critical failure heights. It is found that the commonly used circular slip surface need not be the critical slip surface, especially in non-homogeneous soil slopes. For most practical cases, it is established that the most critical aspect in determining the factor of safety of a slope lies in the accuracy of the soil profile and the soil parameters in each stratum rather than the method of analysis. Some problems associated with slope stability computations such as numerical difficulties in convergence are also discussed.

Introduction

Slope failure has always been one of the major concerns for the geotechnical engineer. Since 1936, many theories have been developed for slope stability analysis based on the method of slices and limit equilibrium analysis. With the advancement of computer technology, the tedious and repetitive computations involved in the analyses can be carried out with relative ease. However, it is not unexpected that these methods of analysis yield different values of factor of safety for a particular slope problem. The objectives of the present work are to compare the factors of safety obtained from various methods based on a few field case studies of test embankments built to critical failure heights, and to examine various theories with regard to assumptions, problems of numerical difficulties, shape of slip surface, number of slices and computing time required.

Limit Equilibrium Methods

Limit equilibrium concept is extensively used in conventional stability analyses of slopes. The approaches most commonly used include the Fellenius (1936), Janbu (1954), Bishop (1955), Morgenstern and Price (1965), and Spencer (1967, 1973) methods. In all these methods, the potential slip surface is divided into a number of vertical slices, and the external and internal forces acting on individual slices are accounted as shown in Fig. 1, where W = weight of slice material, k = seismic coefficient, E = horizontal thrust, X = vertical shear force, P = normal force at slip surface, S_m = mobilised shear

¹Senior Lecturer, ²Associate Professor, ³Former Student, Department of Civil Engineering, National University of Singapore.

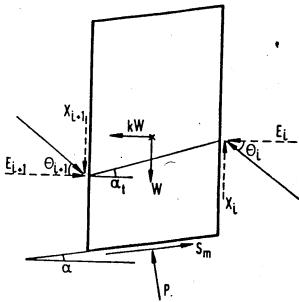


Fig. 1.- Forces acting on an individual slice.

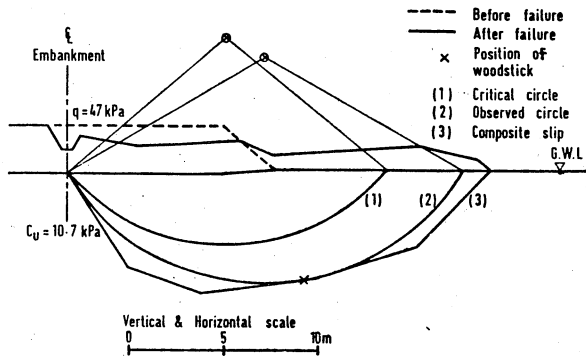


Fig. 2.- Case Study on test embankment on Bangkok Clay (Test Section A)

resistance, θ = inclination of the resultant of interslice force, α_t = inclination of line of thrust and α = inclination of the base of the slice, all angles being measured with respect to the horizontal. The methods differ in the assumptions involving stresses within the slice and the statics employed in deriving the equations leading to the factor of safety. The assumptions and principle of these methods have been highlighted by Chowdhury (1978) and Huang (1983). A comparison of the above methods was presented by Fredlund et al. (1977, 1981) and Duncan and Wright (1980). Fredlund et al. further suggested that the factor of safety of the above methods can be expressed either in terms of overall moment or overall force equilibrium.

Sarma (1973) proposed an approach involving the magnitude of critical horizontal acceleration required to bring the soil mass of the slip surface and the free surface to a state of limiting equilibrium. This critical acceleration was used as a measure of safety.

Law and Lumb (1978) applied the limit equilibrium method to study progressive failure in slope stability under long term condition. They assumed that local failure would occur for an individual slice if the shear stress due to the effect of gravity and pore pressure has exceeded the maximum available shear strength. Once the local failure occurs, it was assumed that the soil resistance would drop abruptly to the final post-peak or residual strength. This then initiates a redistribution of interslice forces and leads to further local failure. Thus a realistic available strengths along the slip surface can be evaluated. Law and Lumb further introduced a new definition for safety factor which is defined as the ratio of the overall shear strength available

to the actual shear strength required for equilibrium.

Marques and Martins (1985) divided the potential slip surface into blocks which were then subjected to Coulomb's failure criterion. Using limit equilibrium, a set of linear equations was derived in terms of horizontal and vertical force equilibrium and moment equilibrium of individual blocks. A linear programming problem was then formulated by considering the equilibrium of the elements and the compatibility of displacements through the duality rules of the mathematical linear programming method such as that proposed by Luenberger (1972).

An overview of the above methods of analysis is given in Table 1.

TABLE 1.- An Overview of Various Methods of Analysis

Methods	Shape of slip surface	Equilibrium conditions satisfied				Number of unknowns
		overall moment	ind. slice moment	vert. force	horiz. force	
Fellenius	circular	yes	no	no	no	1
Bishop simplified	circular	yes	no	no	no	2
Bishop rigorous	circular	yes	no	yes	no	1
Morgenstern & Price	composite	yes	yes	yes	yes	3N *
Spencer (1967)	circular	yes	no	yes	no	1
Spencer (1973)	composite	yes	yes	yes	yes	3N
Janbu simplified	composite	yes	no	yes	yes	2N
Janbu rigorous	composite	yes	yes	yes	yes	3N
Sarma	composite	yes	yes	yes	yes	3N
Law & Lumb	composite	yes	yes	yes	yes	3N
Marques & Martins	composite	yes	yes	yes	yes	3N+1

* N = number of slices

Comparison of Factors of Safety

In the present work, a comprehensive computer program was coded to include all the above limit equilibrium methods of analysis on slope stability. Three published case studies were then used to evaluate the safety factors obtained from these methods. These three case studies are test embankments built to failure on soft clay or silt. Hence their factor of safety at failure is critical and very close to unity. The potential slip surface is also identified in each case. Such data and relevant soil properties measured in-situ greatly enhance the reliability of comparison of different methods of analysis.

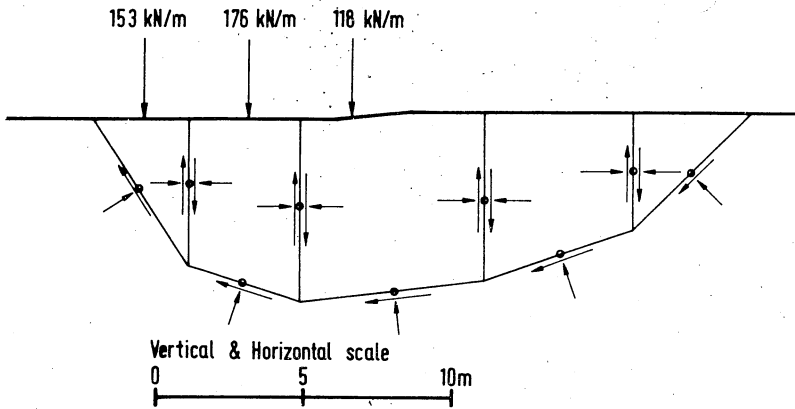


Fig. 3.- Forces Acting on Blocks in Accordance with Marques & Martins (1985) Approach

Case Study 1 : Test embankment on Bangkok clay (Eide and Holmberg, 1972)

This case study is concerned with three test embankments built on soft Bangkok clay to examine the embankment stability for the construction of a highway. All the test embankments were constructed with berms on the right hand side slope in order to ensure that the slope failures would take place to the left hand side where no berms were built. All three sections were 75m long and the slopes 2 vertical to 1 horizontal. Soil profile and properties of a typical section are shown in Fig. 2. The shear strength of soft clay used in the analysis was obtained by field vane tests before the filling.

During tests, filling was carried out until a critical height approached. Failure occurred several days afterwards and frequent measurement of settlements and pore water pressures was made during this period. Sliding zone was identified by means of brittle wood sticks installed prior to failure and it was assumed that failure would cause the brittle wood sticks to break at a depth corresponding to the failure zone. Two of the test sections have been re-analysed and the results are presented in this paper.

For test section A, only one wood stick was recovered and hence only one position of the slip surface can be identified. Based on a slip surface that passes through the observed point as shown in Fig. 2, the factors of safety using various methods are determined as listed in Table 2. Forces acting on the blocks in accordance with Marques and Martins approach are shown in Fig. 3.

TABLE 2.- Results of Case Study on Test Embankments on Bangkok Clay

Methods	Factor of safety				
	Test section A			Test section B	
	(1) critical circle	(2) observed circle	(3) composite slip	(1) critical & observed circle	(2) composite slip
Fellenius	1.35	1.59	-	1.51	-
Bishop simplified	1.42	1.48	-	1.58	-
Bishop rigorous	1.49	1.55	1.08	1.60	1.07
Morgenstern & Price	1.50	1.56	1.10	1.62	1.09
Spencer (1967)	1.51	1.56	-	1.62	-
Spencer (1973)	1.51	1.56	1.10	1.63	1.10
Janbu rigorous	1.55	1.54	1.08	1.61	1.07
Sarma	1.51	1.57	1.08	1.51	1.08
Law & Lumb	1.48	1.51	1.00	1.48	1.00
Marques & Martins	-	-	1.02	-	1.03

It is seen that the factors of safety obtained from various methods do not vary significantly. Although failure occurred in the test embankment, the factors of safety obtained in all the methods are well above unity. In addition, analyses based on other slip circles were also performed and the critical slip circle is established as the one with the lowest factor of safety. The critical circle is practically the same for all the methods except for Fellenius circle which was observed to be displaced slightly. The values so obtained are also given in Table 2 and are about 5% lower than those obtained using the field observed slip circle. The higher computed factor of safety, well above unity, was attributed by Eide & Holmberg (1972) to the higher shear strength of the soft Bangkok clay measured at a large strain-rate and the principle stress orientation along the failure surface. The analysis based on composite (non-circular) slip surfaces using the computer program developed in the present work gives a much lower safety factor for the critical composite surface as shown in Table 2. The values obtained for all the methods with the same strength parameters of clay are close to unity and this shows that the actual failure surface is likely to be non-circular.

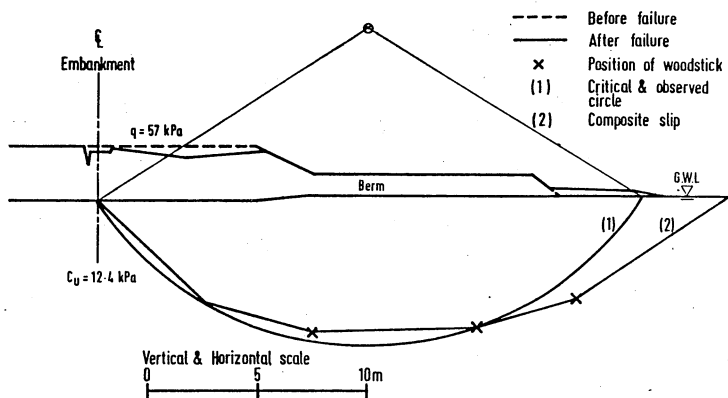


Fig. 4.- Case Study on Test Embankment on Bangkok Clay (Test section B)

For test section B (Fig. 4) where there are berms to both sides of the embankment, three positions along the failure surface were identified by wood sticks. The factors of safety obtained for various methods based on an observed slip circle passing through the three positions are also given in Table 2. In fact this slip circle is subsequently confirmed to be the critical slip circle for all the methods. However, the computed factors of safety are still well above unity for this circle. Further analysis using composite slip surfaces again shows a much lower safety factor for all the methods (Table 2). This further verifies that the critical slip surface need not be circular. It is also found that the critical slip surface passes through the three observed slip positions.

Case Study 2 : Test embankment on sensitive clay (Ladd, 1972)

A test embankment on soft very sensitive clay was constructed to failure in New Hampshire to investigate the in-situ behaviour of the clay. Photographic evidence at site showed that the failure surface was a circular arc and the original 4:1 slope became essentially horizontal after failure. Soil profile and properties according to Ladd (1972) are reproduced in Fig. 5. The shear strength of the soil was based on field vane test data. The factor of safety obtained using circular and composite slip surfaces for the methods are given in Table 3. It is found that all methods yielded nearly identical factors of safety all below unity, indicating failure conditions in the embankment. In addition, the factor of safety using composite slip surfaces is found to be only about 3% lower than that using circular slip surface.

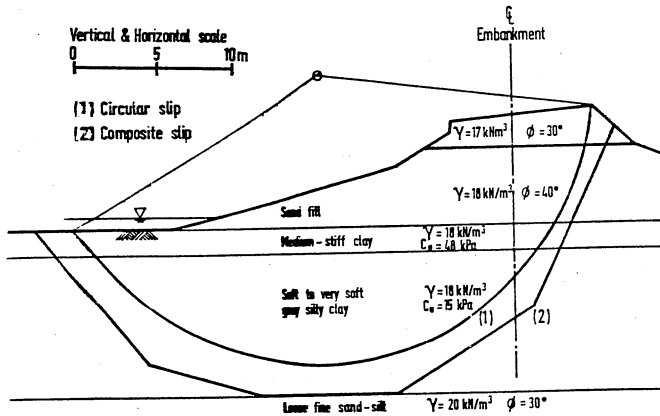


Fig. 5.- Case Study on Test Embankment on Sensitive Clay

TABLE 3.- Results of Case Studies on Test Embankments on Sensitive Clay and Silt

Methods	Factor of safety			
	Embankment on sensitive clay (case study 2)		Embankment on silt (case study 3)	
	(1) circular slip	(2) composite slip	(1) circular slip	(2) composite slip
Fellenius	0.84	-	1.09	-
Bishop simplified	0.92	-	1.14	-
Bishop rigorous	0.93	0.89	1.15	0.98
Morgenstern & Price	0.94	0.90	1.16	0.98
Spencer (1967)	0.94	-	1.16	-
Spencer (1973)	0.94	0.91	1.16	0.97
Janbu simplified	0.91	0.91	1.03	0.93
Janbu rigorous	0.98	0.93	1.21	1.01
Sarma	0.97	0.91	1.17	0.96
Law & Lumb	1.00	1.00	1.12	1.00
Marques & Martins	-	0.88	-	0.98

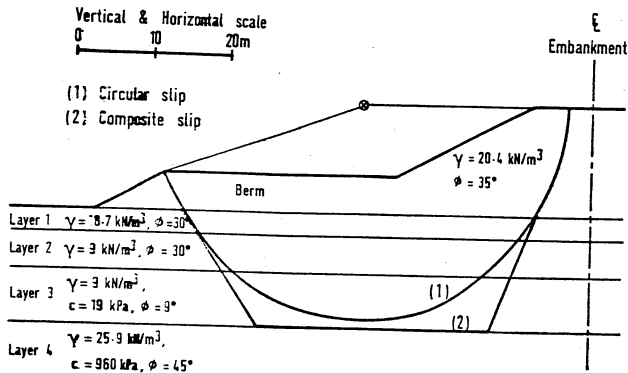


Fig. 6.- Case Study on Embankment on Silt

Case Study 3 : Embankment failure on soft silt (Haupt and Olson, 1972)

An embankment failure occurred during the construction of a highway in Fair Haven, Vermont. Soil profile and properties of this site are reproduced in Fig. 6. The factors of safety obtained by various methods using circular and composite slip surfaces are also given in Table 3. It clearly illustrates that the slip surface is composite in nature, having the form similar to that shown in Fig. 6 as the safety factors are close to 1.

Dicussion

Minimum factors of safety: In most of the cases, it can be seen that the Fellenius method gives the smallest factor of safety among all the methods employed. The assumption that the resultant interslices are parallel to the base leads to an underestimation of the factor of safety as compared to the more rigorous methods. The inaccuracy is also large for deep critical slip surfaces with large variation in base angle. Duncan and Wright (1980) reported that the Fellenius method may give a factor of safety 50% smaller than the other methods, if used for effective stress analysis with high pore pressure.

It appears that Bishop simplified method gives a factor of safety which is less than the rigorous methods by about 1% to 5%. This method is therefore adequate enough for most practical purposes given its simplicity and the time needed for computation. Ting (1983) has noted that a significant error may be inadvertently introduced in estimating the factor of safety due to the approximations used for computing the area and base inclination of each slice. The error is largest for deep slip circles of primarily cohesive slopes. Care

should also be taken in hand computation using a small number of slices as it may lead to unconservative estimates of the factor of safety.

In general, the Janbu simplified method underestimates the factor of safety by as much as 5% to 20%. This is mainly because, as in the first estimate of the Janbu rigorous method, it neglects the interslice shear forces and as a result the factor of safety is normally too conservative. Hence the Janbu simplified method can be used as a quick determination of the safety factor in a preliminary design.

The more rigorous methods, due to Morgenstern and Price, Spencer, Janbu rigorous and Sarma methods, give almost the same factor of safety which is slightly bigger than the value obtained by Bishop simplified method. They are reasonable only when their respective interslice forces are reasonably close to the actual values and when the thrust lines are in the physically admissible region. Reasonable assumptions can be inferred either from a knowledge of the approximate internal stress distribution or from field observation of the internal stresses.

For the limit equilibrium method involving progressive failure by Law and Lumb (1978), the factor of safety obtained is slightly less than those obtained from the above rigorous methods. This is probably due to its ability to pass the interslice forces from a failing slice to a non-failing slice. As a result the shear forces developed at the base of each slice could be slightly larger than the other rigorous methods. The method of Morgenstern and Price using post and peak strengths gives two sets of factor of safety which form the upper and lower bounds for the result using the Law and Lumb method. This reveals that it is often too conservative to use residual strength and too liberal to use peak strength if the soil has undergone considerable straining.

The force optimisation method due to Marques and Martins (1985), allows all the interslice forces to be calculated. In addition, it can be used on a micro-computer and the method uses the Simplex linear programming approach which is both popular and readily available.

As the factors of safety obtained from various methods do not vary significantly, it can be deduced that in most cases the uncertainties related to the definition of geometry and soil properties are greater than those which arise from the approximations involved in the analytical techniques.

Shape of slip surface: Very often, a circular slip surface is assumed in slope stability calculations for reasons of simplicity and convenience. However, the slip surface in non-homogeneous soil is seldom circular, as proven in the case studies. Attempts have been made to identify the actual shape of slip surface and it appears the actual shape is unique and is dependent on the soil profile and properties of each site.

Besides composite slip surfaces, the possibilities of non-circular slips can also be investigated by assuming the slips to be logarithmic or elliptical.

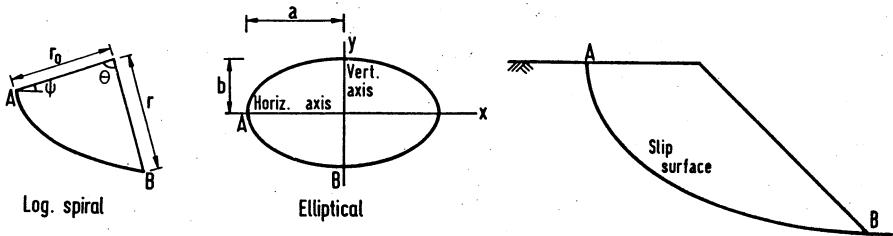


Fig. 7.- Logarithmic Spiral and Elliptical Failure Slip Surfaces

TABLE 4.- Results of Logarithmic Spiral and Elliptical Failure Surfaces

(a) Logarithmic spiral slip surface

Spiral angle (deg.)	-3	-2	-1	0	1	2	3
Entry x(m)	30.6	31.2	31.7	32.2	32.7	33.2	33.6

Methods	Factor of safety						
	Morgenstern & Price	0.894	0.961	1.037	1.257	1.225	1.345
Spencer (1973)	0.895	0.962	1.035	1.122	1.224	1.348	1.491
Janbu simplified	0.801	0.871	0.947	1.135	1.135	1.225	1.397
Janbu rigorous	*	1.031	1.106	1.294	1.293	1.413	1.559

(b) Elliptical slip surface

Horizontal semi axis a(m)	14.62	14.87	15.12	15.37	15.87	16.37	16.87
Vertical semi axis b(m)	17.92	16.89	16.06	15.37	14.30	13.49	12.87

Methods	Factor of safety						
	Morgenstern & Price	0.973	1.014	1.061	1.117	1.233	1.340
Spencer (1973)	*	*	1.060	1.118	1.235	1.342	1.437
Janbu simplified	0.870	0.906	0.949	1.000	1.121	1.241	1.321
Janbu rigorous	1.054	1.099	1.150	1.210	1.315	1.351	1.543

* Non-convergence

Based on a homogeneous soil slope of very soft clay, the factors of safety obtained using the Morgenstern and Price, Spencer and Janbu methods are shown in Fig. 7 and Table 4 respectively. As expected, a circular slip surface gives the lowest factor of safety compared with the positive values of spiral angle for logarithmic spiral slip. However, when negative spiral angle is used, the factor of safety decreases until non-covergency occurs. If the soil strength is allowed to increase substantially, it appears that circular slip surfaces would give the lowest factor of safety regardless of positive or negative magnitude of spiral angle for all the four methods of analysis. Similar phenomenon is observed for elliptical slip surfaces.

Total and effective stress analysis: It is often critical to know when total or effective stress analysis is required for excavation or construction of an embankment. The guiding criterion seems to be the degree of dissipation of construction pore pressure. The usual procedure is to adopt a total stress analysis in saturated low permeability soils immediately after construction and an effective stress analysis in all other cases with appropriate drained values of soil properties. For some over-consolidated clays, the residual parameters $c_r = 0$ and ϕ_r may have to be used at large strain conditions. It is often important to identify the most critical condition in any practical problem in order that the appropriate shear strength parameters are used in design.

TABLE 5.- Results of Example Problem from Fredlund and Krahn (1977).

Methods	Factor of safety		
	without peizometric line		with peizometric line
	$r_u = 0$	$r_u = 0$	
Fellenius	1.288	1.029	1.171
Bishop simplified	1.372	1.124	1.245
Bishop rigorous	1.370	1.122	1.241
Morgenstern & Price	1.378	1.124	1.230
Spencer (1967)	1.378	1.218	1.245
Spencer (1973)	1.370	1.115	1.240
Janbu simplified	1.443	1.191	1.533
Janbu rigorous	1.430	1.162	1.298
Sarma	1.450	1.161	1.295
Law & Lumb	1.512	1.170	1.280

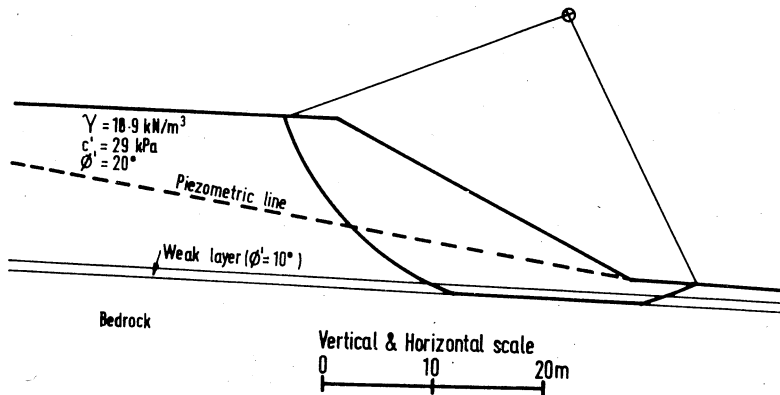


Fig. 8.- Example Problem on Effective Stress Analysis from Fredlund & Krahn (1977).

Based on an example given in Fredlund and Krahn (1977) and shown in Fig. 8, the stability of a non-homogeneous slope in terms of effective stress parameters are re-analysed using the present computer program and the results are given in Table 5. Fellenius method gives the lowest value of factor of safety while the values obtained from the other methods do not differ significantly except that the value obtained from Janbu simplified method gives relatively higher value of safety factor.

Numerical difficulties: Occasionally there exists a problem due to non-convergence of the factor of safety for most of the rigorous methods. Chowdhury (1978) attributed this difficulty to large changes in horizontal side forces in successive iterations as a result of the large variation of soil properties in stratified soil. In the Morgenstern and Price method, the force and moment conditions cannot be satisfied simultaneously and as in the Spencer methods, this can be explained by the extremely different inter-slice forces introduced by soil properties of stratified layers.

The shape of the slip surface seems to affect the Janbu rigorous method most critically since it uses the value of parameter m_α for computation. The m_α is basically a function of $\tan \phi$ and $\tan \phi'/F$ where α is the inclination of the base of a slice and ϕ' is the effective angle of friction. Computational difficulties occur when m_α becomes small or zero, when α is negative and $\tan \phi'/F$ is large, or when α is large and $\tan \phi'/F$ is small. Moreover, the computed factor of safety may be negative when a particular slice has a small but negative m_α value. Ching and Fredlund (1983) reported that problems associated with the magnitude of m_α are

mainly the result of an inappropriately assumed shape of the slip surface. The assumed surface form can cause conditions that give unreasonable m_{α} values in the numerical procedure. They further suggested that the inclination of the slip surface in the active and passive zones of the sliding mass should be limited to magnitudes of $(45 + \phi/2)^{\circ}$ and $(45 - \phi/2)^{\circ}$ respectively so as to reduce the problem of non-convergency due to m_{α} .

Ching and Fredlund also reported that the calculation of interslice forces may sometimes present difficulties in the stability computation. In most limit equilibrium methods of slices, an interslice force assumption is made to render the stability problem tractable. Generally, these assumptions are related to the direction or point of application of the interslice forces. Although it is possible to employ a wide range of assumptions on possible interslice forces, unreasonable solutions or non-converging conditions can result if the assumptions are unrealistic. Numerical difficulties may arise and as a result the method of analysis may not yield a satisfactory solution.

When the slice width is varied, the factor of safety seems to converge in a random manner. However, on closer observation, it is realised that this is due to the different interslice forces as a result of different slice width. This is pertinent especially where the slope consists of strata with widely varying soil parameters.

TABLE 6.- Factor of Safety for Different Number of Slices.

Number of slices	8	16	32	64	128
Method	Factor of safety of a homogeneous soil slope				
Fellenius	1.437	1.441	1.447	1.449	1.450
Bishop simplified	1.511	1.519	1.521	1.521	1.521
Morgenstern & Price	1.526	1.530	1.538	1.538	1.538
Spencer (1973)	1.527	1.531	1.538	1.539	1.539
Janbu rigorous	1.517	1.527	1.531	1.533	1.533

The effect of the number of slices on the factor of safety of a homogeneous soil slope was checked as shown in Table 6. It is observed that the factor of safety increases as the number of slices increases but there is little improvement once the number of slices exceeds about 30. Spencer (1967) suggested that there is no advantage in taking the number of slices above 32. In addition, it is noticed that as the number of stratified layers is increased, the number of slices required to reach a steady factor of safety also increases.

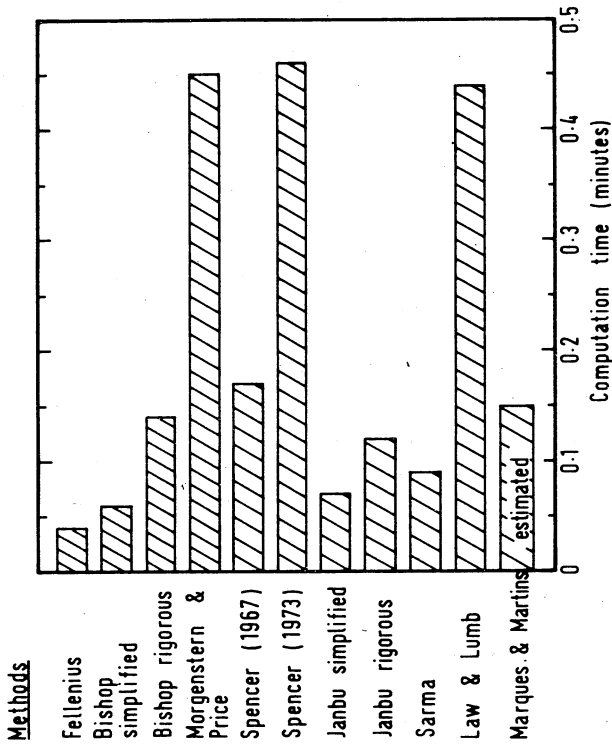


Fig. 9.- Computation Time for Various Methods.

Computation time: Computation time for various methods for the Bangkok clay case (section A) is shown in Fig.9 using the IBM 3081 mainframe computer system. The Bishop simplified method needs 0.06 min for each stability analysis and the Fellenius method required approximately 60% of that time. The longest computation time of 0.45 min is for the Morgenstern and Price (1965), Spencer (1973), and Law and Lumb (1978) methods. However, when computing a factor of safety for methods which require a known interslice force distribution, the time taken can be much longer since this force distribution, has to be obtained on a trial and error basis. In the case of force optimisation approach of Marques and Martins, the computation was carried out on a 128K RAM personal computer for a length of 33 minutes.

Conclusion

From three case studies, it has been established that the factors of safety obtained using various methods of analysis based on limit equilibrium, with exception of the Fellenius method, do not vary significantly. However, the commonly used circular slip surface is found to be inappropriate for a number of case studies where a composite slip surface, determined by soil stratification, is more realistic. Problems associated with slope stability computation such as numerical difficulties in convergence have been discussed in detail. It is also deduced that for most practical cases, the most critical aspect in determining the factor of safety of slope lies in the accuracy of the soil profile and the soil parameters in each stratum rather than the method of analysis.

Acknowledgements

The authors wish to thank the assistance of Teo Yen Pai and Hoo Kwai Seng, former students of the Department of Civil Engineering, National University of Singapore, for coding and running the computer programs as a part of a research project.

Appendix I - References

1. Bishop, A.W. (1955). The use of slip circle in the stability analysis of slopes. *Geotechnique*, Vol.5, pp.7-17.
2. Ching, R.K.H. & Fredlund, D.G. (1983). Some difficulties associated with the limit equilibrium method of slices. *Canadian Geotechnical Journal*, Vol.20, pp.661-672.
3. Chowdhury, R.N. (1978). *Slope Analysis. Development in Geotechnical Engineering*, 22, Elsevier Scientific Publishing Company, Amsterdam.
4. Duncan, J.M. & Wright, S.G. (1980). The accuracy of equilibrium methods of slope stability analysis. *Engineering Geology*, Vol.16, pp.5-17.
5. Eide, O. & Holmberg, S (1972). Test fills to failure on the soft Bangkok Clay. Proc., Speciality Conf. on Performance of Earth and Earth-supported Structures, ASCE, Vol.1, part 1, pp.159-180.
6. Fellenius, W. (1936). Calculation of the stability of earth dams. Proc., Second Congress on Large Dams, No.4, pp.445-463.
7. Fredlund, D.G., Krahn, J. (1977). Comparison of slope stability methods of analysis. *Canadian Geotechnical Journal*, Vol.14, pp.429-439.
8. Fredlund, D.G., Krahn, J. & Pufahl, D.E. (1981). The relationship between limit equilibrium slope stability methods. Proc., 10th Int. Conf. on Soil Mech. and Found. Engrg., Stockholm, Vol.3, pp.409-416.
9. Haupt, R.S. & Olson, J.P. (1972). Case history - embankment failure on soft varved silt. Proc., Speciality Conf. on Performance of Earth and

- Earth-supported Structures, ASCE, Vol.1, Part 1, pp.1-27.
10. Huang, Y.H. (1983). Stability Analysis of Earth Slopes. Van Nostrand Reinhold, New York.
 11. Janbu, N (1954). Application of composite slip surface for stability analysis. Proc., European Conf. on the Stability of Slopes, Stockholm, Vol.3, pp.43-49.
 12. Ladd, C.C. (1972). Test embankment on sensitive clay. Proc., Speciality Conf. on Performance of Earth and Earth-supported Structures, ASCE, Vol.1, Part 1, pp.101-128.
 13. Law, K.T. & Lumb, P. (1978). A limit equilibrium analysis of progressive failure in the stability of slopes. Canadian Geotechnical Journal, Vol.15, pp.113-122.
 14. Luenberger, D.G. (1972). Introduction to Linear and Nonlinear Programming, Addison-Wesley, Reading, USA.
 15. Marques, P.S. & Martins, J.B. (1985). Safety factor of slopes by linear programming in a microcomputer. Proc., Int. Conf. on Education, Practice and Promotion of Computational Methods in Engrg. using Small Computers, Macau, Vol.2A, pp.221-229.
 16. Morgenstern, N.R. & Price, V.E. (1965). The analysis of the stability of general slip surfaces. Geotechnique, Vol.15, pp.79-93.
 17. Sarma, S.K. (1973). Stability analysis of embankments and slopes. Geotechnique, Vol.23, No.3, pp.423-433.
 18. Spencer, E. (1967). A method of analysis of the stability of embankments assuming parallel interslice forces. Geotechnique, Vol.17, pp.11-26.
 19. Spencer, E. (1973). Thrust line criterion in embankment stability analysis. Geotechnique, Vol.23, pp.201-215.
 20. Ting, J.M. (1983). Geometric concerns in slope stability analysis. Journal of Geotechnical Engineering, ASCE, Vol.109, No.11, pp.1487-1491.

THE SELECTION OF THE MOST APPROPRIATE MODEL FOR 1-D CONSOLIDATION

By Tennekoon. B.L.¹

ABSTRACT: A large number of theories for consolidation have been published but their verification with field results has been found to be extremely difficult. The paper presents a simple alternative method for the selection of the most appropriate model for consolidation. It is proposed that laboratory consolidation tests be carried out where both settlements and pore pressures are measured. These measurements are then made use of by first determining the constants for any model using the 'settlement-time' curve, and then predicting the 'pore pressure-time' curve. The predicted and measured 'pore pressure-time' curves are then compared to obtain the most appropriate model for a particular clay. The use of this method is illustrated with an example selecting five models of consolidation for study viz. Terzaghi (1925), Gibson and Lo (1961), Barden (1968), Bjerrum (1967) and Christie and Tonks (1985).

Introduction

The first rational theory to explain the settlements occurring in saturated clays was the 1-D theory of consolidation proposed by Terzaghi, (Terzaghi, 1925). One of the main advantages of the theoretical model for consolidation is that it becomes possible to carry out laboratory consolidation tests on thin samples of clay, a few centimeters thick (with an increment of load normally kept on for 24 hours), and then from the laboratory results predict the settlements in the field where the clay layer may be several meters thick, and where the settlements may take place over a long period of time.

When verifying the predictions from Terzaghi's theory in the field, two major discrepancies have been observed: viz.

- (i) settlements continue to take place even after the excess pore water pressures have dissipated; and
- (ii) the measured rate of settlement and the measured rate of pore pressure dissipation in the field is faster than the predicted rates.

Consequently, many studies have been made to develop alternative theories for consolidation. Most of these are modifications to Terzaghi's original theory, although a few distinct theories have also been proposed.

¹Professor of Civil Engineering, University of Moratuwa, Sri Lanka

For example, theories have been developed removing the assumption of Terzaghi that the coefficient of permeability of the soil is constant (Barden, 1965a; Davis and Raymond, 1965; Barden and Berry, 1965; Poskitt, 1969; Berry and Poskitt, 1972; Samarasinghe, 1986).

Theories have been developed for the soils where the strains are not small (Gibson and Hussey, 1967; Poskitt, 1969; Berry and Poskitt, 1972; Mesri and Rokhsar, 1974; Samarasinghe, 1986).

There are theories in which the constitutive equation of Terzaghi has been modified to take into account the observed soil creep (Gibson and Lo, 1961; Lo, 1961; Barden 1965b, Barden, 1968; Barden, 1969).

There are a few theories which could be classified as being fundamentally different from the Terzaghi theory. The theory of Bjerrum (1967) and variations of this (Bent Hassen, 1969; Garlanger, 1972; Christie and Tonks, 1985) belong to this category. Other alternative models have also been proposed (Mesri and Choi, 1985; Hanrahan, 1973).

When confronted with all these theories, there could be confusion as to which would be the most appropriate model that could be used to predict the consolidation behaviour of a clay. It is noted that in the use of all these theories, the soil constants for a model are first obtained by curve fitting to the laboratory 'settlement-time' curve; and then these constants are used with the model to predict field behaviour. In the final analysis, the validity of the model depends on how good these field predictions are. Unfortunately, the testing of a model by comparing the predicted and measured field settlements nearly always run-up against three main problems; viz.

- (i) the time duration over which accurate field measurements have to be made is often quite long;
- (ii) thick layers of soil in the field are often anisotropic and non-homogeneous and
- (iii) drainage conditions in the field may be two or three dimensional.

In this context an alternative approach is desirable to select the most appropriate consolidation model for a clay.

Constitutive Equation in Consolidation

Since one dimensional settlement results from the compression of voids(e), the settlement(s) of a clay layer can be computed from

$$s = \sum \left\{ \frac{\Delta e}{1 + e_0} \right\} \cdot \Delta H \quad (1)$$

where the summation is to be carried out over all the soil layers, e_0 is the initial voids ratio in the layer, and ΔH is the thickness of the soil element layer

Hence, the settlements can be computed from Eq.1 if the constitutive equation for the soil, i.e. the $(e - \sigma' - t)$ relationship for the soil, can be established. The aim of all the models of consolidation is to derive such a relationship.

A detailed study of the different theories of consolidation shows that there are two distinctive approaches to develop the constitutive equation in consolidation. The first, termed the 'rheological approach', attempts to model the observed settlement behaviour in clays by various combinations of springs and dashpots. In the other approach, termed the 'analytical approach', the observed settlement behaviour is directly modelled mathematically.

Some Rheological Models for the Constitutive Equation

In the rheological approach, various combinations of springs and dashpots are used to model the observed settlement behaviour. The springs and the dashpots may be ascribed as either linear or non-linear properties. Three such examples are shown in Fig.1.

The Terzaghi model (Terzaghi, 1925) shown in Fig. 1a is a linear spring for which the constitutive equation is

$$\frac{de}{d\sigma'} = - a_v = \text{constant} \quad (2a)$$

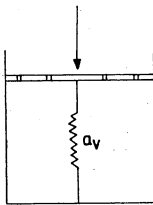


Fig.1a - Terzaghi Model

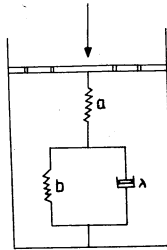


Fig.1b-Gibson and Lo Model

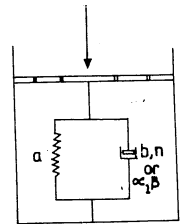


Fig.1c- Barden Model

Fig. 1.- Some Rheological Models of Consolidation

The Gibson and Lo model (Gibson and Lo, 1961) is shown as Fig. 1b. In this model, all the elements are assumed linear with the top spring (constant = a) representing primary consolidation behaviour, and the bottom spring (constant = b) and dashpot (constant = λ) representing secondary consolidation behaviour. The resulting constitutive equation has been determined as

$$e = a \cdot \sigma'(t) + \lambda \int_0^t \sigma'(\tau') \cdot e^{-\frac{\lambda}{b}(t-\tau')} \cdot d\tau' \quad (2b)$$

where τ represents a dummy variable.

Barden has proposed a rheological model (Barden, 1965b, and Barden, 1969) as shown in Fig. 1c, where the 'primary consolidation spring' used by Gibson and Lo has been eliminated but non-linearity has been introduced into the dashpot. The resulting constitutive equation could be written as

$$\frac{e - e_f}{a} = \tau + u \quad (2c - 1)$$

where e_f = the final voids ratio,

e = the linear compressibility of the spring, and

τ = the viscous resistance of the dashpot

Barden introduced non-linearity into the dashpot by writing its equation as

$$(i) \quad (\tau)^n = b \cdot \left(\frac{\partial e}{\partial t} \right) \quad (2c-2) \text{ (Barden, 1965b)}$$

where 'n' is greater than 1, or

$$(ii) \quad \frac{\partial e}{\partial t} = \beta \sinh(\alpha \tau) \quad (2c-3) \text{ (Barden, 1968)}$$

Some Analytical Models for the Constitutive Equation

In his Rankine Lecture, Bjerrum discussed the consolidation settlements which occur in a normally consolidated clay such as Drammen clay (Bjerrum, 1967). He proposed that such clays undergo 'ageing' and that when an 'aged' clay is loaded the settlements which occur can be separated into two parts - an 'instant compression' occurring with an increase in effective stress, and a 'delayed compression' taking place at unchanged effective stress. This is shown graphically in Fig. 2a.

This behaviour can be expressed mathematically (Bent Hansen, 1969) as

$$\Delta e = C_r \cdot \log_{10} \left(\frac{P_c}{P_o} \right) + C_c \cdot \log_{10} \left(\frac{P_f}{P_c} \right) + C_a \cdot \log_{10} \left(\frac{t_i + t}{t_i} \right) \quad (3a)$$

where P_o , P_f are the initial and final soil pressures respectively,
 t_i is the time associated with the 'instant time line',
 P_c is the critical pressure of the soil corresponding to the 'instant time line',

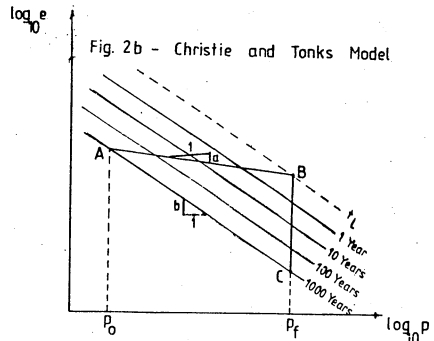
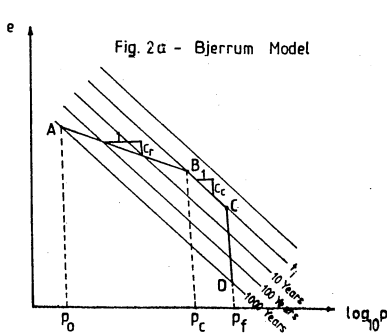


Fig.2.- Some Analytical Models of Consolidation

- c_r = slope of $(e - \log_{10} p)$ line for $p < p_c$,
 c_c = slope of $(e - \log_{10} p)$ line for $p > p_c$, and
 c_a = slope of $(e - \log_{10} t)$ line.

Bent Hansen has also suggested the re-formulation of Eq. (3a) by assuming linear relationships in doubly logarithmic space, thus giving

$$\Delta(\log_{10} e) = a \log_{10} \left(\frac{p_c}{p_0} \right) + b \log_{10} \left(\frac{p_f}{p_c} \right) + C \log_{10} \left(\frac{t_i + t}{t_i} \right) \quad (3b)$$

where a , b and c replace the earlier soil constants c_r , c_c and c_a respectively.

A modification to the Bjerrum model has been proposed (Christie and Tonks, 1985) where the t_i line is done away with, and a new limit time line t_L corresponding to Fig. 2b is introduced. The major advantage of this modification is that the new model thus requires one less parameter for its definition. The constitutive equation for this model is

$$\Delta(\log_{10} e) = a \cdot \log_{10} \left(\frac{p_f}{p_0} \right) + C \cdot \log_{10} \left(\frac{t_i + t}{t_i} \right) \quad (3c)$$

A Method for the Selection of the Most Appropriate Model for Consolidation

It is proposed that laboratory consolidation tests involving the measurement of both the settlement and the pore pressures at different times be carried out. Different models for consolidation can then be tested by first determining the soil constants for the model by curve fitting to the 'settlement-time' curve and then using these soil constants to predict the 'pore pressure-time' curve for the laboratory sample. It will then be assumed that the model which gives the best fit for the 'pore pressure-time' curve is the most appropriate model for consolidation for that particular clay.

This method will be illustrated with reference to some test results reported on remoulded Grangemouth clay (Christie and Tonks, 1985). This clay is a post-glacial estuarine mud which has been formed after the last glaciation in the Forth Valley of Scotland. In the tests reported by Christie and Tonks, the samples have been first saturated by the application of back pressure, and the consolidation tests have been carried out with increments of load kept on for as much as 7 days. Measurements have also been made of the pore pressure at the base of the sample.

Figs. 3a and 3b show the variation of the voids ratio and the pore pressure at the base with time for a typical test in which,

$$e_o = \text{initial voids ratio} = 0.940$$

$$H = \text{initial sample thickness} = 20 \text{ mm}$$

$$P_o = \text{initial stress acting on sample} = 120 \text{ kN/m}^2$$

$$\Delta p = \text{stress increment} = 120 \text{ kN/m}^2$$

The pore pressure (u) at the base of the sample as in Fig. 3b been expressed non-dimensionally as μ_b where $\mu_b = u/\Delta p$

Determination of the Constants for the Model, and the Prediction of the Variation of Pore Pressure with Time

In this section, five models for consolidation with different constitutive equations have been chosen for study. They are the Terzaghi model (Terzaghi, 1925), the Gibson and Lo model (Gibson and Lo, 1961), the Barden model (Barden, 1965b), the Bjerrum model (Bjerrum, 1967), and the Christie and Tonks model (Christie and Tonks, 1985).

1. The Terzaghi Model

- (a) The soil constants for this model were determined by the standard Taylor's method and found to be

$$c_v = 1.62 \text{ mm}^2/\text{min}; m_v = 3.958 \times 10^{-4} \text{ m}^2/\text{kN}$$

- (b) The variations of e and μ_b with time were obtained as follows:

- (i) for any time t , the time factor T is computed as

$$T = \frac{C_v t}{H^2}$$

- (ii) the degree of consolidation (U) is calculated as

$$\bar{u} = 1 - \frac{8}{\pi^2} \sum_{n=0}^{\infty} \left[\frac{1}{(2n+1)^2} \cdot \exp. \left\{ -(2n+1)^2 \frac{\pi^2 T}{4} \right\} \right]$$

$$\text{and hence } e = e_o - U (\Delta e)$$

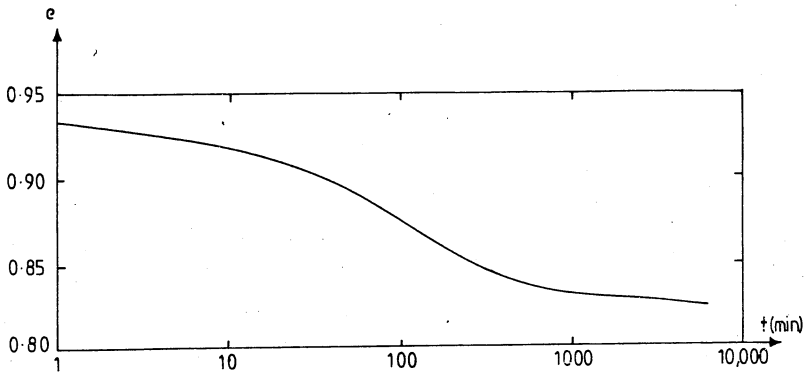


Fig. 3a.- Experimental Settlement - Time Relationship

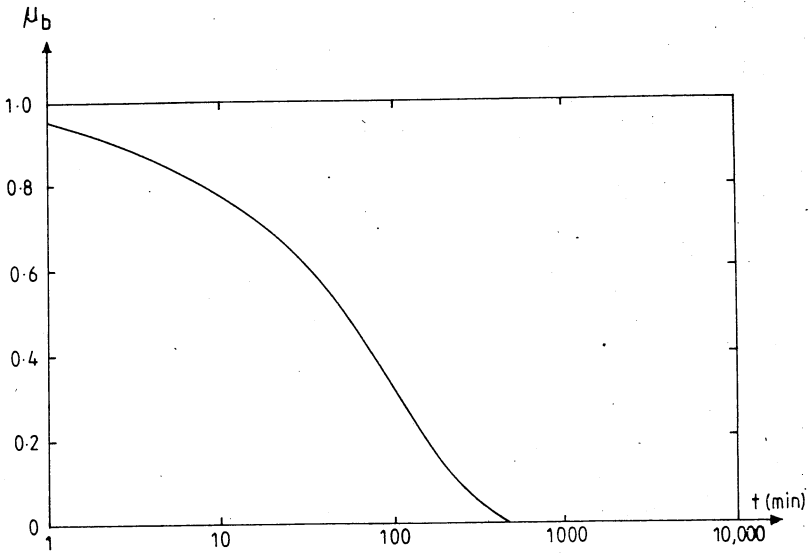


Fig. 3b.- Experimental pore pressure - Time Relationship

Fig. 3.- Experimental Results of Christie and Tonks (1985) for sample of Grangemouth Clay with following Parameters:

Amount of ageing = 7 days, $e_o = 0.940$, $H = 20\text{mm}$,
 $p_o = 120\text{kN/m}^2$, $\Delta p = 120\text{kN/m}^2$

where Δe is the total change in voids ratio during the load increment.

- (iii) the dimensionless pore pressure at the base (u_b) is calculated as

$$u_b = \frac{4}{\pi} \sum_{n=0}^{\infty} \left[\frac{1}{(2n+1)} \cdot \sin \frac{(2n+1)\pi}{2} \exp \left\{ - (2n+1)^2 \cdot \frac{\pi^2 T}{4} \right\} \right]$$

The predicted results are compared with the observed values in Figs. 4a and 4b. The major drawbacks in the Terzaghi model are observed as

- (a) soil creep is not taken into account; and
 (b) the measured pore pressure dissipation is much faster than the predicted.

2. The Gibson and Lo Model

- (a) The soil constants (a, θ) corresponding to the primary consolidation phase and (b, λ) corresponding to the secondary consolidation stage were initially determined as recommended by Lo, (Lo, 1961).

This gave

$$a = 5.464 \times 10^{-4} \text{ m}^2/\text{kN}; \quad b = 1.049 \times 10^{-4} \text{ m}^2/\text{kN}$$

$$\theta = 0.8919 \text{ mm}^2/\text{min}; \quad \lambda = 0.166 \times 10^{-8} \text{ m}^2/\text{kN per min.}$$

The corresponding non-dimensional parameters M, N (Christie, 1964) worked out as

$$M = \frac{a + b}{a} = 1.92$$

$$N = \frac{\lambda H^2}{b\theta} = 0.0071 \text{ for the 20mm thick sample}$$

- (b) The variations of e and u_b with time were obtained as follows:

- (i) for any time t , the time factor T is computed as

$$T = \frac{\theta t}{H^2}$$

(ii) the degree of consolidation (\bar{U}) is calculated as (Christie, 1964)

$$\bar{U} = 1 + \frac{8}{\pi^2} \sum_{n=0}^{\infty} \left[\frac{1}{(2n+1)^2} \cdot f_1(T) \right]$$

$$f_1(T) = \left[\frac{(2n+1)^2 \pi^2}{M} - \frac{1}{\bar{x}_1} \right] \exp\left(-\frac{\bar{x}_2 T}{4}\right) - \left[\frac{(2n+1)^2 \pi^2}{M} - \frac{1}{\bar{x}_2} \right] \exp\left(-\frac{\bar{x}_1 T}{4}\right)$$

$$\frac{\bar{x}_1}{\bar{x}_2} = \frac{1}{2} \left[4MN + (2n+1)^2 \pi^2 \pm \sqrt{\{4MN + (2n+1)^2 \pi^2\}^2 - 16N(2n+1)^2 \pi^2} \right]$$

Hence, $e = e_0 - U(\Delta e)$

(iii) the dimensionless pore pressure at the base is calculated as

$$u_b = \frac{4M}{\pi^3} \sum_{n=0}^{\infty} \left[\frac{1}{(2n+1)^3} \cdot \sin(2n+1) \frac{\pi}{2} \cdot f_2(T) \right]$$

where

$$f_2(T) = \left[\frac{(2n+1)^2 \pi^2}{M} - \frac{1}{\bar{x}_2} \right] \exp\left(-\frac{\bar{x}_1 T}{4}\right) - \left[\frac{(2n+1)^2 \pi^2}{M} - \frac{1}{\bar{x}_1} \right] \exp\left(-\frac{\bar{x}_2 T}{4}\right)$$

When the above soil constants were used, it was found that the settlements in the primary stage were being over-predicted. Therefore, the parameter 'a' alone was varied (keeping b, θ and λ unchanged) until the best fit was obtained for the 'settlement-time' curve. The value so obtained was $a = 4.561 \times 10^{-4} \text{ m}^2/\text{kN}$; and these new soil constants were used to obtain the predicted 'voids ratio-time' and 'pore pressure-time' curves shown in Figs. 4a and 4b.

It is observed that when compared to the Terzaghi model, there is now better agreement for the 'settlement-time' curve. However, the observed pore pressure dissipation is still much faster than predicted by the Gibson and Lo model.

3. The Barden Model

(a) The solution for the Barden model is illustrated using the equation of the dashpot as

$$(\tau)^n = b \cdot \left(\frac{\partial e}{\partial t} \right)$$

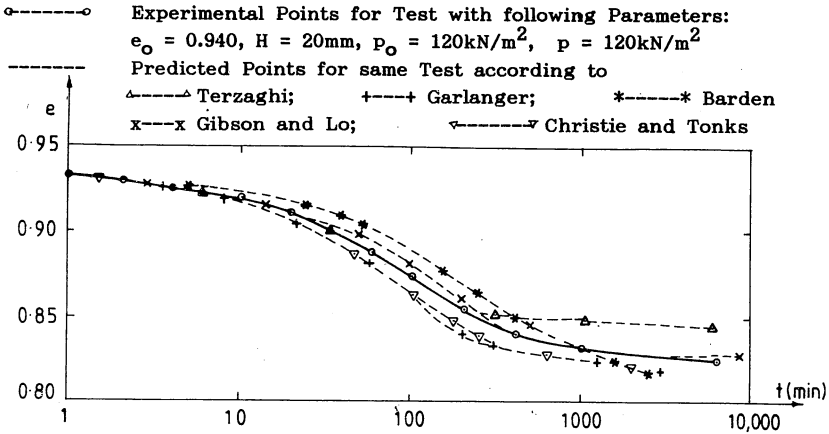


Fig. 4a.-Comparison of Measured and Predicted Variation of Settlement with Time

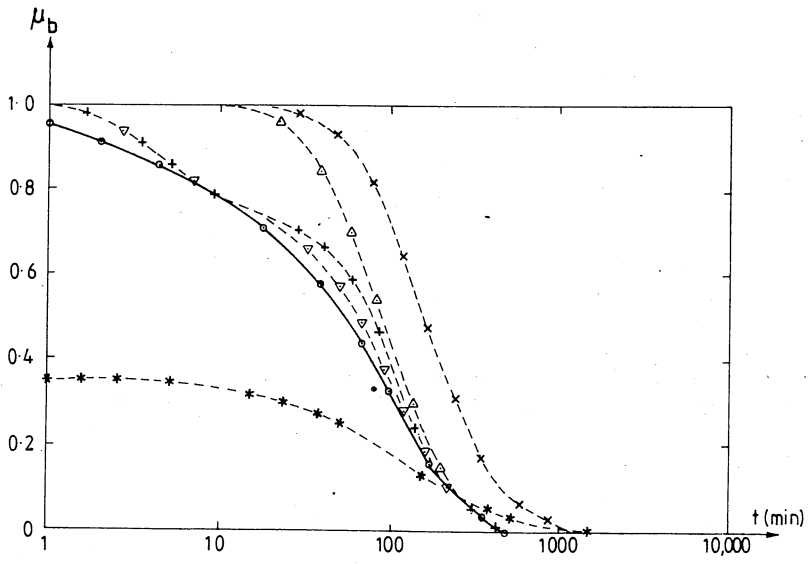


Fig. 4b.- Comparison of Measured and Predicted Variations of Pore Pressure with Time

Barden obtained a solution for the variation in the degree of consolidation and the pore pressure with time (Barden, 1965b) in terms of n and a new soil parameter R defined by

$$R = \frac{T}{T_s} = \left(\frac{C_v}{H^2} \right) \times \left(\frac{t}{T_s} \right)$$

T being the time factor governing the diffusion process, and T_s being the time factor associated with the structural viscosity of the soil.

The ratio (t/T_s) has to be computed by curve fitting the creep part of the 'settlement-time' curve to a set of theoretical curves obtained by Barden.

The soil constants so obtained were

$c_v = 1.62 \text{ mm}^2/\text{min.}$; $n = 5$ and $(t/T_s) = 561 \text{ min.}$
giving a value of $R = 0.2268$ for the sample of thickness 20mm.

(b) The variations of e and μ_D with time were obtained as follows:

(i) The time t is related to the time factor T by

$$T = \frac{C_v t}{H^2}$$

(ii) The average degree of consolidation and the dimensionless pore pressure at the base were determined by writing a computer program for the solution of the two simultaneous equations obtained by Barden for any consolidating layer; viz.

$$\frac{\partial^2 \mu}{\partial x^2} = \frac{\partial \lambda}{\partial T}$$

$$\text{and} \quad \frac{\partial \lambda}{\partial T} = \frac{1}{R} (\lambda - \mu)^n$$

$$\text{where} \quad \mu = \frac{u}{\Delta P}$$

$$= 1 - (\text{degree of consolidation of the layer})$$

$$x = Z/H, H \text{ being the length of the drainage path}$$

The above differential equations were written in finite difference form and an implicit method of solution (Poskitt, 1967) was used. In this method of solution, truncation errors are the major problem. In space dimensions, these were kept satisfactorily by the use of 10

elements, i.e. 11 nodes. The next problem is the choice of the time step. For equations of this type, a logarithmic increase in time steps using empirically determined constants have been found to give results to reasonable accuracy.

$$\text{Defining } (tx) = \log_{10} T \quad (4a)$$

$$\text{It was found that the use of } (tx)^+ = (tx) + \Delta(tx) \quad (4b)$$

$$\text{with } (tx)_0 = -3.025 \text{ and } \Delta(tx) = 0.025 \quad (4c)$$

gave results to the same accuracy as that given by Poskitt. Hence, this computer program was used to obtain the results shown in Figs. 4a and 4b.

It is seen that the Barden model predicts a very rapid initial dissipation of pore pressure for the laboratory sample, but this has not been observed experimentally.

4. The Bjerrum Model

- (a) The mathematical form of the constitutive equation for the Bjerrum model was given as equations (3a) and (3b). These equations can be reformulated into a form from which numerical solutions can be obtained (Garlanger, 1972).

The soil constants a , b and c , as well as the t_i value have to be determined from special consolidation tests (Christie and Tonks, 1985). The soil constants so obtained were

$$\begin{aligned} a &= 0.018, & b &= 0.216, & c &= 0.0067 \\ t_i &= 0.9185 \text{ min.} & & & & \text{and } c_v = 1.62 \text{ mm}^2/\text{min.} \end{aligned}$$

- (b) The variation of e and μ_b with time were obtained as follows:

- (i) The time t is related to the time factor T by

$$T = \frac{c_v t}{H^2}$$

- (ii) The average degree of consolidation and the dimensionless pore pressure at the base were determined by writing a computer program for the solution of two simultaneous equations obtained by Garlanger for any consolidating layer; viz.

$$\frac{\partial^2 \mu}{\partial x^2} = - \frac{\partial \beta}{\partial T}$$

$$\text{and } \frac{\partial \mu}{\partial T} = \frac{\left(\frac{\partial \beta}{\partial T}\right) - \left(\frac{\partial \beta}{\partial T}\right)}{\left(\frac{\partial \beta}{\partial \mu}\right)}$$

where β = degree of consolidation of the layer,
 μ = dimensionless pore pressure of the layer,

and $\left(\frac{\partial \beta}{\partial T}\right)_p$ is related to the creep rate at constant effective stress.

The finite difference approximations to the derivatives, and the method of computing $\left(\frac{\partial \beta}{\partial T}\right)_p$ are given by Garlanger. In the computer program which was developed, a semi-implicit scheme of solution was used with the consolidating layer divided into 10 elements, and time steps selected according to Equations (4a), (4b), and (4c).

It is observed that the predicted pore pressure distribution is very similar to the measured distribution.

5. The Christie and Tonks Model

- (a) The mathematical form of the constitutive equation for the model was given as Equation (3c).

The soil constants are the same as for the Bjerrum Model, but this model requires one parameter less for its definition.

The soil constants obtained are,

$$a = 0.018 ; b = 0.216 \quad c = 0.0067$$

and $c_v = 1.62 \text{ mm}^2/\text{min}$.

- (b) The variations of e and μ_b with time were obtained using the same equations obtained by Garlanger for the Bjerrum Model. The equation for the the creep rate $\left(\frac{\partial \beta}{\partial T}\right)_p$ is however modified according to the new assumptions for the model (Christie and Tonks, 1985). The predicted pore pressure distribution is found to be very similar to that predicted by the Bjerrum model, and very close to the measured distribution.

Conclusions

A method is proposed for the determination of the most appropriate model for 1-D consolidation of a clay. It is proposed that laboratory consolidation tests be carried out in an oedometer where readings are taken of the variations of both settlement and pore pressure with time. Different theoretical models are then tested by first determining the soil constants for

the model by curve fitting to the 'settlement-time' curve; and then these soil constants together with the model are used to predict the laboratory 'pore pressure-time' curve. It is proposed that the model which gives the best agreement between the measured and predicted curves of 'pore pressure-time' would be the most suitable model for predicting the consolidation behaviour of the clay.

This approach has been illustrated with an example on some laboratory test results on remoulded Grangemouth clay (Christie and Tonks, 1965). Five models of consolidation, viz. Terzaghi; Gibson and Lo; Barden; Bjerrum; and Christie and Tonks; were tested with the experimental results. The paper describes the methods which could be used to,

(i) determine the soil constants from the 'settlement-time' curve; and

(ii) predict the variation of pore pressure with time, for each of this models.

TABLE 1.- Soil Constants used for Analysis

MODEL	SOIL CONSTANTS
Terzaghi	$c_v = 1.62\text{mm}^2/\text{min}$. $m_v = 3.958 \times 10^{-4}\text{m}^2/\text{kN}$
Gibson and Lo	$a = 4.561 \times 10^{-4}\text{m}^2/\text{kN}$, $\theta = 0.8919\text{mm}^2/\text{min}$. $b = 1.049 \times 10^{-4}\text{m}^2/\text{kN}$, $\lambda = 0.166 \times 10^{-8}\text{m}^2/\text{kN per min}$.
Barden	$c_v = 1.62\text{mm}^2/\text{min}$. $R = 0.2268$, $n = 5$ (and $\Delta e = 0.170$)
Bjerrum	$a = 0.018$, $b = 0.216$, $c = 0.0067$ $c_v = 1.62\text{mm}^2/\text{min}$. $t_i = 0.9185 \text{ min}$.
Christie & Tonks	$a = 0.018$, $b = 0.216$, $c = 0.0067$ $c_v = 1.62\text{mm}^2/\text{min}$.

The soil constants obtained for the remoulded Grangemouth clay are given in Table 1. It is shown that for this clay, the Bjerrum model and the Christie and Tonks model both give very similar results (for the variation of pore pressure with time) which are very close to the observed results. Thus either of these models could be selected as the most appropriate model for 1-D consolidation for this clay.

Acknowledgments

The work described in this paper was carried out at the University of Edinburgh, U.K. during the tenure of a Commonwealth Staff Fellowship awarded by the Association of Commonwealth Universities. The Author wishes to thank Prof. A.W. Hendry, Professor and Head of the Department of Civil Engineering and Building Science at the University of Edinburgh for his support and encouragement. Thanks are also due to Dr.I.F. Christie, Senior Lecturer in Civil Engineering at the University of Edinburgh, for many stimulating discussions, and for granting permission to quote from the experimental results in the paper (Christie and Tonks).

Appendix I - References

1. Barden, L. (1965a). Consolidation of compacted and unsaturated clay. *Geotechnique* Vol.15, 267-286.
2. Barden, L. (1965b). Consolidation of clay with non-linear viscosity. *Geotechnique* Vol.15, 345-362.
3. Barden, L. (1968). Primary and secondary consolidation of clays and peat. *Geotechnique* Vol.18, 1-24.
4. Barden, L. (1969). Time dependent deformation of normally consolidated clays and peats. *Journal of Soil Mechanics and Foundation Division, ASCE*, Vol.95(1), 1-31.
5. Barden, L. and Berry, P.L. (1965). Consolidation of normally consolidated clay. *Journal of Soil Mechanics and Foundation Division, ASCE*, Sept. 1965, SM5, 15-35.
6. Bent Hansen (1969). A mathematical model for creep phenomena in clay. *Proc. of Speciality Session No.12 on Advances in Consolidation Theories for Clays*. 7th ICSMFE Mexico, 12-18.
7. Berry, P.L. and Poskitt, T.J. (1972). The consolidation of peat. *Geotechnique* Vol.22, No.1, 22-52.
8. Bjerrum, L. (1967). Engineering geology of Norwegian normally consolidated marine clays as related to the settlement of buildings. *Geotechnique* Vol.17, No.2, 81-118.
9. Christie, I.F. (1964). A re-appraisal of Merchant's contribution to the theory of consolidation. *Geotechnique* Vol.14, 309-320.
10. Christie, I.F. and Tonks, D.M.(1985). Developments in the time lines

- theory of consolidation. Proc. on 11th ICSMFE, San Francisco, Vol.2, 423-426.
11. Davis, E.H. and Raymond, G.P. (1965). A non-linear theory of consolidation. Geotechnique Vol.15, 161-173.
 12. Garlanger, J.E. (1972). The consolidation of soils exhibiting creep under constant effective stress. Geotechnique Vol.22, No.1, 71-78.
 13. Gibson, R.E. and Hussey, M.J.L. (1967). The theory of one dimensional consolidation of saturated clays. Geotechnique Vol.17, No.3, 261-273.
 14. Gibson, R.E. and Lo, K.Y. (1961). A theory of consolidation of soils exhibiting secondary compression. Acto polytechnica Scandinavica, 296/1961.
 15. Hanrahan, E.T. (1973). The stress-strain relationship in Soil Mechanics. Civil Eng. Public Works Review, January 1973.
 16. Lo, K.Y. (1961). Secondary compression of clays. Journal of Soil Mechanics and Foundation Division, ASCE, Vol.87, SM4, August 1961, 61-87.
 17. Mesri, G. and Choi, Y.K. (1985). The uniqueness of the end of primary void ratio-effective stress relationship. Proc. of 11th ICSMFE, San Francisco, Vol.2, 587-590.
 18. Mesri, G. and Rokhsar, A. (1974). Theory of consolidation for clays. Journal of the Geotechnical Engineering Division, ASCE, Vol.100, No.GT8, August 1974, 889-904.
 19. Poskitt, T.J. (1967). A note on the consolidation of clay with non-linear viscosity. Geotechnique Vol.17, 284-289.
 20. Poskitt, T.J. (1969). The consolidation of saturated clay with variable permeability and compressibility. Geotechnique Vol.19, No.2, 234-252.
 21. Samarasinghe, A.M. (1986). An evaluation of one-dimensional consolidation of soils. Proc. of Symposium on Geotechnical Problems and Practices in Foundation Engineering, Colombo. 258-268
 22. Terzaghi, K. (1925). Erdbaumechanik. Vienna, F. Deuticke.

Appendix II - Notations

The following symbols are used in the paper :

e	- void ratio
e_o	- initial void ratio
e_f	- final void ratio
Δe	- change in void ratio
p	- vertical effective stress
p_o	- initial vertical effective stress
p_f	- final vertical effective stress
p_c	- critical vertical effective stress (Bjerrum, 1967)
Δp	- change in vertical effective stress
s	- settlement

t	- time
t_i	- time associated with instant time line (Bjerrum, 1967)
t_L	- time associated with limit time line (Christie and Tonks, 1985)
(Δt)	- time step for implicit method of solution
(Δt) ₀ , Δt	- empirical constants used to define time step for implicit method of solution
u	- excess pore water pressure (Pore pressure)
x	- length along drainage direction measured non-dimensionally (= z/H)
z	- length along drainage direction
H	- length of drainage path in consolidating layer
ΔH	- thickness of element of consolidating layer
R	- soil parameter (= T/T _g) (Barden, 1965b)
T	- time factor associated with diffusion process (T = c _v t/H ²)
T _g	- time factor associated with the structural viscosity of the soil (Barden, 1965b)
\bar{U}	- average degree of consolidation
β	- degree of consolidation (Garlanger, 1972)
λ	- (1-degree of consolidation) (Barden, 1965b)
μ	- dimensionless pore pressure (= u/ Δp)
μ_b	- dimensionless pore pressure at base
σ	- vertical effective stress (effective normal stress)
τ	- viscous resistance of dashpot (Shear stress)
ϵ	- strain associated with consolidation (Linear strain)
a_v, c_v, m_v	- soil constants for Terzaghi model
a, b, θ, λ	- soil constants for Gibson and Lo model
M, N	- alternate non-dimensional soil parameters corresponding to Gibson and Lo model.
b, n	- soil constants for Barden model (Barden, 1965b)
α, β	- alternate soil constants for Barden model (Barden, 1969)
c_r, c_c, c_e	- soil constants for Bjerrum model
a, b, c	- alternate soil constants for Bjerrum model as well as for the Christie and Tonks model

DESIGN ASPECTS OF THE DEEP GROUT CURTAIN - RANDENIGALA DAM

By Gunasekera. A.U¹

ABSTRACT : Geotechnical Investigations conducted during the feasibility studies and subsequently prior to tender stage of Randenigala Project revealed the existence of joint patterns (formed mainly as a result of regional tectonism) in the bed rock forming the dam foundations, which will facilitate water seepage from the reservoir. Thus to control and minimize water seepage referred to above a "Deep Grout Curtain" was designed to be constructed by injecting cement grout under various pressures appropriate to localities and elevations through boreholes drilled in a certain pattern.

The paper deals with the Engineering Geologic conditions of the Randenigala Dam foundation (core trench) very briefly but the design aspects of the deep grout curtain are elaborated in detail, and also recommendations for execution are given.

Introduction

Randenigala Hydro Power Project Site is located in the valley of river Mahaweli between Victoria Dam and Minipe anicut (about 5.4km upstream of Minipe anicut) about 35km South-East of Kandy.

The river bed elevation at Randenigala Site is approximately 148m MSL. This project (both stages Randenigala and Rantembe) once completed is expected to meet one fifth of the country's present electrical energy demand in addition to the regulation of water supply for irrigation purposes to downstream irrigation schemes of systems A, B and C.

The project consists of a hundred and two (102m) metre high rockfill dam with a central clay core, Chute Spillway, Power House, Power Intake with steel lined Power Tunnel, Irrigation Outlet and other adjacent structures.

The estimated total cost of the project is about 520 million DM.

For Main Project Data see table No.1.

Engineering Geologic Conditions of the Dam Foundation - Core Trench

Bed Rock: The core trench area is constituted by intermediate granulitic gneiss of which the main mineralogical components are quartz, feldspar and pyroxene. Gneissic Structure is not well pronounced but can be observed in

¹Section Engineer, Materials & Foundations - Randenigala Project
Central Engineering Consultancy Bureau

TABLE 1.- Main Project Data

MAIN PROJECT DATA

GENERAL

MAXIMUM FLOOD LEVEL	236.2 m	MSL
RETENTION LEVEL	232.0 m	MSL
DRAWDOWN LEVEL	22.0 cm	MSL
NORMAL TAILWATER LEVEL	152.0 m	MSL
CATCHMENT AREA	23.50	km ²
RESERVOIR CAPACITY (AT RETENTION LEVEL)	860	MCM
ACTIVE STORAGE (FOR DRAWDOWN LEVEL)	270	MCM
RESERVOIR SURFACE AT RETENTION LEVEL	23.5	km ²
WATED CROSS HEAD	80	m
WATED NET HEAD (APPROXIMATELY)	77.8	m
WATED DISCHARGE	80	m ³ /s

MAIN DAM

CREST ELEVATION	239.0 m	MSL
RIVERBED ELEVATION (APPROXIMATELY)	148.0 m	MSL
MAXIMUM HEIGHT OF DAM	102.0 m	MSL
VOLUME OF DAM	3.7	MCM
FREEBOARD AT RETENTION LEVEL	7.0	m
CREST LENGTH (APPROXIMATELY)	485	m
MAXIMUM BASE WIDTH	298	m

SPILLWAY

DESIGN CAPACITY	4550	m ³ /s
MAXIMUM CAPACITY	8086	m ³ /s
CREST ELEVATION	218.0 m	MSL
NUMBER OF BATES	3	
TYPE OF BATES	TAINTOR	
HEIGHT OF BATES	15.24	m
WIDTH OF BATES	18.70	m
TOTAL WIDTH OF WEIR CREST	60	m
TOTAL WIDTH OF CHUTES (3x18.0m)	48.0	m
LENGTH OF CHUTE No. 1	225.8	m
No. 2	231.8	m
No. 3	237.8	m

BOTTOM AND IRRIGATION OUTLET

INTAKE TOWER

DIAMETER OF OVERFLOW LIP	14.00	m
DIAMETER OF VERTICAL SHAFT	9.60	m
ELEVATION OF OVERFLOW LIP	170.0 m	MSL
TUNNEL DIAMETER BETWEEN INTAKE TOWER & BATE CHAMBER	9.60	m
TUNNEL LENGTH BETWEEN INTAKE TOWER & BATE CHAMBER	220	m
NUMBER OF SERVICE BATES	2	TAINTOR
TYPE OF SERVICE BATES	2	
NUMBER OF REVISION BATES	~284	m ³ /s
TYPE OF REVISION BATES	~315	m ³ /s
CAPACITY AT DRAWDOWN LEVEL		
CAPACITY AT RETENTION LEVEL		

POWER INTAKE AND WATERWAYS

HEIGHT OF POWER INTAKE (APPROXIMATELY)	80 m
SILL ELEVATION AT INTAKE	179.30 m MSL
DISCHARGES AT EL 232.0 m MSL	2x90.0 m ³ /s
AT EL 220.0 m MSL	2x92.2 m ³ /s
AT EL 203.0 m MSL	2x70.1 m ³ /s
BELOW EL 203.0 m MSL	Turbines closed
LENGTH OF PENSTOCK (APPROXIMATELY)	270 m
LENGTH OF MANIFOLD (APPROXIMATELY)	40 & 50 m (respectively)
DIAMETER OF PENSTOCK	6.20 m
DIAMETER OF MANIFOLD	3.90 m

POWER HOUSE

NUMBER OF UNITS	2
TYPE OF TURBINES	FRANCIS
SETTING OF TURBINES	148.50 m MSL
INSTALLED CAPACITY (AT GENERATED TERMINALS)	2x81 MVA

certain localities. Generally, an equigranular, granulitic fabric is predominant which results in a quite compact and thick banded to massive appearance. Fine, medium and coarse grained rock types (without much of a difference in mineralogical composition) grade into each other without sharp borders of different mineral contents.

Further, a few very thin biotite schist bands, striking N-S in conformity with foliation of regionally developed gneiss with nearly vertical dipping occur on the right bank and the river bed sections. (See Engineering Geological map of Core trench - Fig. 1).

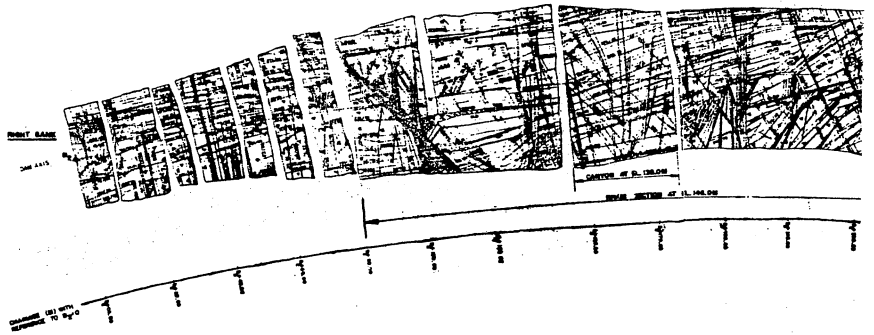
Foliation: The foliation planes, being the planes of separation between one layer of minerals and the next, reflect the former bedding planes. The spacing of foliation planes ranges between a few centimeters in scarcely occurring gneissose metasediments and some tens of centimetres and even some metres in massive granulitic gneisses. Orientation of the foliation planes is North-South with a strike maximum at W 353°N to N5°E more or less perpendicular across the river. According to the joint measurements the dip of foliation varies between 80° towards East (downstream) and 82° towards West (upstream).

Fracture Zones and Joints: In the core trench area (see Fig. 1) joints are very well developed and (at this elevation) as observed in the bottom of the core trench where fresh rock occurs they are chloriticized (or healed with a secondary chloritic formation). Where moderately weathered rock occurs with limited extension, near extensively fractured zones these joints are weathered and in some of them even clayey filling was observed.

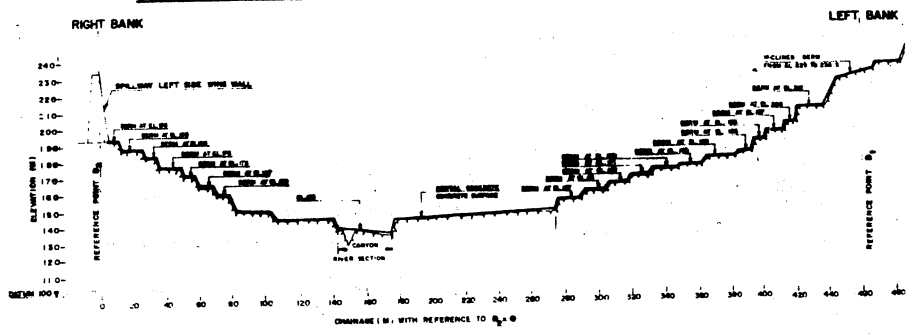
According to the observations and measurements done in the core trench area the following three joint patterns are to be distinguished :

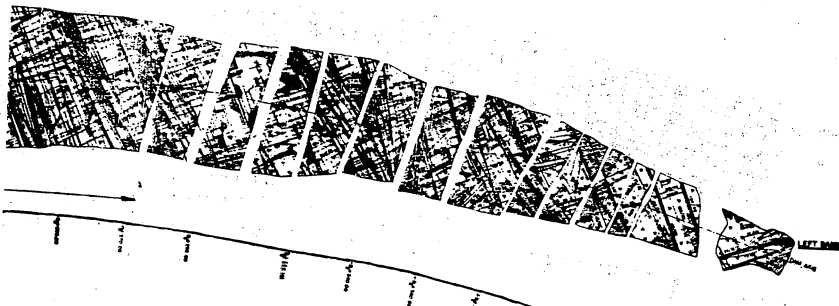
- | | | |
|-------------|---|--------------------------|
| Pattern I | : | Strike : W353°N to N5°E |
| | | dip : 80°E - 90° - 82°W |
| Pattern II | : | Strike : N84°E to E96°S |
| | | dip : 84°S - 90° - 79°N |
| Pattern III | : | Strike : W345°N to N13°E |
| | | dip : 64°W - 90° - 70°E |

Joints of Pattern I represents the foliation planes. The joints of Pattern II reflect the main regionally well developed tectonic feature - the fracture zones with a strike maximum in East-West direction. Dip is vertical or with near vertical angles to South or North. The joints of pattern III cuts the rock mass with more gently inclined angles than foliation planes with dips towards either East or West.

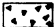
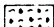
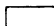



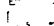
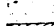
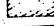
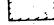
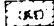




LONGITUDINAL SECTION ALONG THE DAM AXIS (BOTTOM OF THE CORE TRENCH)





LEGEND

-  MODERATELY WEATHERED ROCK.
-  BIOTITE SCHIST
-  FRESH ROCK.
-  JOINT WEATHERED AND FILLED WITH CLAY.
-  JOINT WEATHERED.
-  JOINT CHLORITICIZED
-  JOINT CHLORITICIZED AND SLICKENSIDED
-  JOINT PLANE - WEATHERED.
-  JOINT PLANE - CHLORITICIZED
-  JOINT PLANE - SLICKENSIDED AND CHLORITICIZED
-  FRACTURED ZONE - WEATHERED
(a) WITHOUT CLAY FILL (b) WITH CLAY FILL
-  FRACTURED ZONE - CHLORITICIZED
-  DIP DIRECTION AND DIP ANGLE

NOTES:

DEGREE OF WEATHERING:

DECOMPOSED ROCK: ROCK IS DECOMPOSED AND STRENGTH COMPLETELY LOST, WHEN CHANGED TO SOIL ORIGINAL FABRIC IS PRESERVED, CORE-STONES SCARCE.

HIGHLY WEATHERED: ROCK IS DISCOLOURED DISCONTINUITIES MAY BE OPEN AND HAVE DISCOLOURED SURFACES AND THE ORIGINAL FABRIC NEAR DISCONTINUITIES MAY BE ALTERED ALTERATION STARTS DEVELOPING ALONG THE JOINTS.

MODERATELY WEATHERED: ROCK IS PARTLY DISCOLOURED DISCONTINUITIES MAY BE OPEN AND SURFACES DISCOLOURED WITH ALTERATION DEVELOPED ALONG THE JOINTS

SLIGHTLY WEATHERED: ROCK MAY BE DISCOLOURED PARTICULARLY ADJACENT TO DISCONTINUITIES WHICH MAY BE OPEN AND WILL HAVE SLIGHTLY DISCOLOURED SURFACE. ROCK IS NOT NOTICEABLY WEAKER THAN FRESH ROCK

FRESH ROCK: ROCK IS UNFFECTED BY ANY WEATHERING

Fig. 1.- Engineering Geologic Map of Core Trench

Of the above three joint patterns, the intensity of fracturing reflected by Pattern II is relatively higher in the core trench area and forms two major fracture zones striking more or less East-West from chainage $D_2 + 20$ to chainage $D_2 + 100$ and from chainage $D_2 + 320$ to $D_2 + 390$ (see Fig. 1) which are also observed in the grouting gallery.

Engineering Geologic Investigations

At Randenigala Project site engineering geologic investigations were carried out in three stages as shown below :

Stage I : Feasibility Studies

Nine exploratory boreholes were executed with (NX size) core recovery to depths varying from 60m to 200m with inclinations ranging from 0° (vertical) to 50° . Five of these were on the right bank and the remaining were located on the left bank at different elevations. This programme was carried out from May 1979 to August 1979 and the total meterage of drilling was 923m.

Stage II : Final Designs

Final design stage investigations were executed from September 1979 to February 1980. During this period, twentytwo boreholes were sunk to depths varying from 40m to 100m with inclinations ranging from 0° to 48° . The total meterage of drilling was 1570m. The locations of the drill holes executed during the above mentioned stages are given in Fig. 2.

Also two horizontal test adits were excavated on either abutments as shown on Fig. 2 and they have the following characteristics :

Test adit	Length (m)	Azimuth	Elevation of st. 0.00m at the inlet
Right Bank	75.6	S191°W	175.036
Left Bank	76.0	N25°E	162.579

The overburden and decomposed bed rock were removed by open cut excavation. Having reached sufficient rock cover and rock strength the adits were driven by underground excavation with a more or less square tunnel section (as chosen by the contractor) with 1.80m with. Wooden supports extended from portal to station 35m on the right bank adit and to 23m and additionally from 32 to

35m on the left bank adit thus corresponding to the highly weathered rock zones.

Stage III : Pre Construction (partially during construction period)

Eighteen numbers of exploratory holes with a total meterage of 1414m were drilled along the dam axis to varying depths from 60m to 107m. First eight (No.EHDA 1 to EHDA 8) of them were inclined 15° from the vertical (along the dam axis) towards left bank and the other ten (No.EHDA 9 to EHDA 18) were inclined 20° towards (along the dam axis) Right Bank, as shown on Fig. 2 and Fig. 3. (The purpose of this investigation programme was not only to study the permeability of rock, but also to calculate excavation quantities of rock and soil).

In all the exploratory holes and on cores recovered, the below mentioned tests/recordings by observation were done to investigate the quality of bed rock in respect of permeability of the rock mass :

1. Water pressure tests in drill holes
 2. Recording of core recovery
 3. Calculation of rock quality designation (RQD)
-
1. The permeability of the bed rock has been determined by water pressure tests according to the Lugeon method. The lengths of the test stages were approximately 3m. One complete Lugeon test comprises 5 pressure steps (2-5-10-5-2 bars) in ascending and descending succession. Each pressure step was maintained for 6 minutes (10 minutes if the absorption was low). The obtained water loss (absorption) is expressed in Lugeon (1 Lugeon = water loss in litres per minute and per metre length of tested section in the bore hole under a pressure of 10 bars).
 2. Core recovery as a measure of weakness, disintegration, dissection of the rock mass by joints and fractures etc. has been recorded.
 3. The rock quality designation (RQD) is a criterion of the quality and soundness of the rock mass. For the determination of the RQD the core recovery percentage of pieces of sound core over 10cm long was compiled.

Analysis of Investigation Data

Analysis of investigation results of stage I & II: As mentioned in the preceding section, water pressure tests (Lugeon tests) were performed in exploratory drill holes in order to obtain quantitative permeability characteristics of bed rock in the project area. But this type of tests could not be performed in the upper most geo-strata where overburden, decomposed

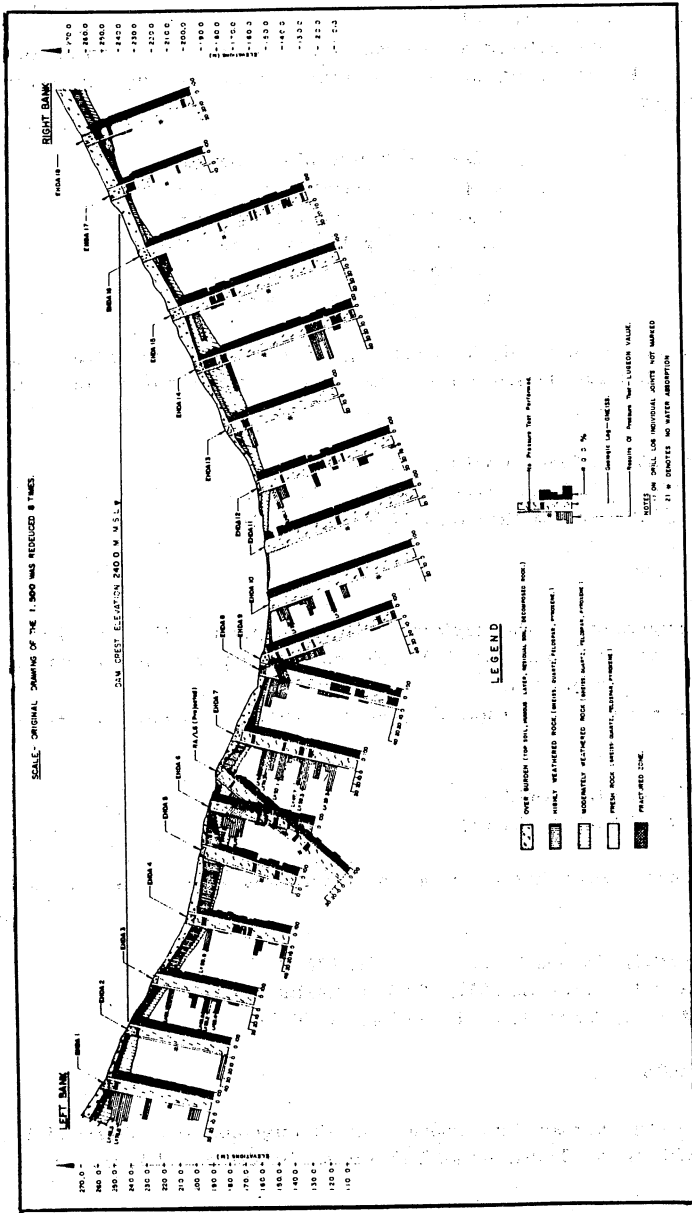


Fig. 3.- Geotechnical Section Along the Dam Axis
Results of Investigations

and highly weathered rock occurred.

In analysing the data related to permeability of rock the following classification of rock according to permeability based on Lugeon value criterion was adopted.

< 1	Lugeon - Technically impervious
1 - 4.9	Lugeon - Moderately permeable
5 - 9.9	Lugeon - Distinctly permeable
10 - 19.9	Lugeon - Highly permeable
20 - 49.9	Lugeon - Very highly permeable
> 50	Lugeon - Extremely permeable

On the Left Bank at Randenigala according to the water pressure tests conducted, very high water losses - more than 20 Lugeons occurred down to depths of :

19.24m (RA/L3), 23.18m (RA/L4), 24.23m (RA/L6),
19.50m (RA/L7), 12.15m (RA/L8), 13.40m (RA/L9),
25.72m (RA/L10), 13.60m (RA/L11), 17.16m (RA/L12).

Average 18.35m

(Note : The designation of the exploratory hole is given within brackets.. The given depths are not along the drill hole but vertical depths calculated, as most of the holes were inclined).

Also highly permeable - more than 10 Lugeon - zones were encountered at depths given below

From 55.20m to 61.1m (RA/L1)
From 80.51m to 83.71m (RA/L3)

On the Right bank very highly permeable rock was encountered at the following depths

20.94m (RA/R1), 19.34m (RA/R2), 14.07m (RA/R3)
15.31m (RA/R4), 7.94m (RA/R7), 20.37m (RA/R9)
20.10m (RA/R10), 7.05m (RA/R14), 46.06m (RA/R17)

Average 19.0m

Below this zone high permeability (more than 10 Lugeons) was observed in boreholes No.RA/R10 up to 38.9m, No.RA/R12 up to 50.08m and RA/R15 up to 44.10m.

PERMEABILITY OF BEDROCK OF THE DAM FOUNDATION

(FROM CHAINAGE D₂-118 TO CHAINAGE D₂+477)

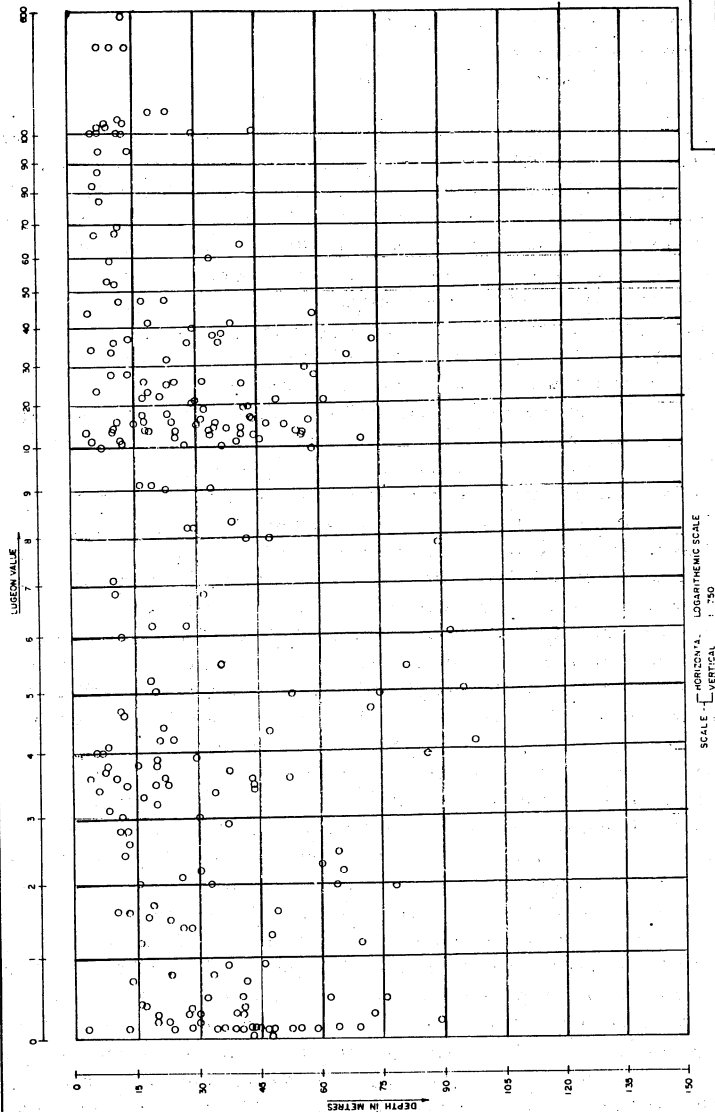


Fig. 4.- Permeability of Bedrock of the Dam Foundation

Further very high to extremely high water losses >20 Lugeon and >50 Lugeon were observed in zones as given below :

From 41.87m to 47.93m (RA/R2)

From 80.23m to 86.38m (RA/R6)

From 73.81m to 100.28 m (RA/R13)

These high permeabilities are directly attributed to the fractured zones encountered by the drill holes as confirmed by RQD measurements and other observations made on recovered cores. In some cases it has been noticed that the results of water pressure tests have not been in conformity with observations made on cores recovered and RQD. Contradicting data such as very low RQD values and low absorption or no absorptions are simply due to the fact that observed fresh chloriticised joints on the core (breakage of core has taken place due to vibration of drilling along weak chloriticised joints of Gneisses, where chlorite is a very weak secondary formation) are tight and consequently non absorbing when in rock mass in-situ.

Further, also consideration should be given to the fact that specially in cases where very high water intakes occurred the pump capacities often were insufficient to carry out the pressure tests with the required accuracy. Hence, it should be expected that the real permeability in such locations would be higher than the given Lugeon values.

On the basis of the test results which were obtained from exploratory drill holes located at Randenigala site (rather scattered covering the whole area) it could be concluded that on both river banks the bed rock has a very highly to highly permeable zone down to a depth of about 40m. Within this, the upper most 20-25m of rock is very highly permeable. (But a part of it about 15-20m will be excavated during the dam foundation because the dam will be founded on moderately weathered or fresh rock and these upper 15-20m of rock stratum includes decomposed and highly weathered rock).

Further, below this ±40m depth there is another ±40m zone in some areas where exploratory holes were executed rock zones with high, very high and extremely high permeabilities too were encountered at depths reaching 70-75m. They are individual zones of limited extension (in the order of a few tens of metres), which can be attributed to major fracture zones. These fracture zones are in conformity with the regional tectonic lineaments.

The exploratory adit on left bank being more or less in the direction of North-South was predominantly crossed by fracture systems of East-West strike. In it a few North-South striking fracture zones too were observed. On the entire length of the adit the observed rock was with closely to very closely spaced joints. In the two major fracture zones (striking East-West) observed joints were with about 10cm spacing predominantly and rarely 5cm.

In the adit on the Right abutment North-South striking joints and fracture zones have been exposed, which were similar to the ones exposed on the Left

Bank.

Both adits were driven to the full length of 75m during the rainy season and a steady water seepage through the joints on the crown as well as on both side walls was observed in both adits along the full length.

The rock portions (in fresh rock, slightly or moderately weathered rock) between fractures were observed to be hard and the joints were - mainly the ones which were open facilitating seepage - without fillings.

Therefore, it could be concluded reliably on the basis of above observations in adits as well as on core samples that the rock, in the foundation would permit seepage of water and can be grouted with cement grout under pressure successfully and satisfactory consolidation as well as tightening will be achieved.

In the light of the above mentioned facts and in conformity with the International Standard Practice of such works it was proposed to consolidate the very highly to highly permeable rock zone (beneath the bottom of the core trench which is 15-20m from ground surface) of the dam foundation - average 40m deep - with a "vertical grout fan" (Fig. 10) consisting of six grout holes executed from the bottom of the core trench and grouting gallery (located at a depth of about 15m below core trench). The fan itself is to be perpendicular to the dam axis and the distance between two consecutive fans is 3m.

In the foundation of the dam, below the above referred to very highly permeable zone i.e. below the grouting gallery, a grout curtain is to be constructed to reach a depth of about 60m from the ground surface. The grout holes are to be inclined in such a way towards LB or RB as to pierce through joints as much as possible making the grouting more effective. The spacing between grout holes to be 6m and in fracture zones where intake will be high the spacing is to be 3m or even 1.5m if so required, depending on the water pressure test results which are to be conducted during execution.

The grouting gallery was located 30--85m from the ground surface below the very highly to highly permeable rock zone, which requires consolidation with "grout fans". For dam (core trench) foundations about 15-20m of soil and decomposed highly weathered rock were expected to be excavated; hence the grouting gallery was to be at a depth of about 15m from the bottom of the core trench.

However, the proposed parameters of the above grout curtain were to be verified and adjusted (if necessary) after the final pre-construction investigation programme. Please refer Stage III Pre-Construction Investigation, which was confined to the dam foundation extending along the dam axis, covering the full length.

Further, the proposed parameters of the grout curtain were finalised after the Pre-Construction (Stage III) investigations, and were checked once again by test grouting (Test grouting programme I and II) executed in a chosen test area in the dam foundation.

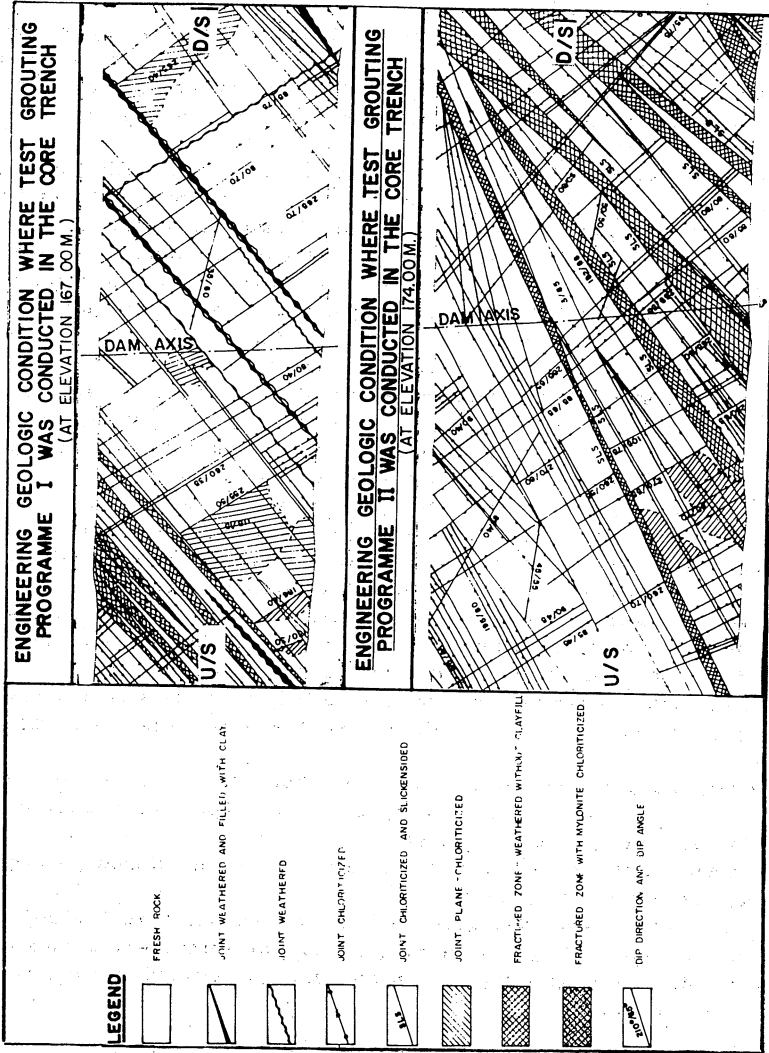


Fig. 5.- Engineering Geologic Condition of the Area under Test Grouting Program

The results of the Stage III investigations are given on Fig. 3 - Geotechnical Section along the Dam Axis. On Fig. 4, the results of all permeability tests conducted in exploratory holes during all three investigation stages, are plotted together.

The results of the final stage investigations giving a very comprehensive picture of the engineering geologic conditions of the dam foundation confirmed the results of the previous investigations. Thus proving that the proposed grout curtain does not require any adjustments or alterations.

Subsequently the test grouting was carried out to finally check the suitability of the proposed grouting programme for the dam foundation.

Test Grouting

The purpose of executing test grouting was :

- a) To verify the effectiveness of the technical parameters assumed for the grout curtain (on the basis of investigation data.
- b) To test efficiency of grouting procedures and equipment.

These grouting tests were performed in two separate programmes which were designed in a manner to simulate as far as possible, the interaction of the expected geological conditions on the dam foundation and the grouting procedure (methodology) to be executed with the available equipment.

The areas for testing have been chosen from a section where the jointing is most intensive according to the Engineering Geologic map of the dam site.

Test Grouting Programme I : For the upper section (consolidation grouting above gallery) of the grout curtain.

The engineering geologic situation of the area subjected to testing between chainages D_2+300 and D_2+320 is shown in Fig. 5. As seen on the map, this area is very intensively fractured - very closely to closely spaced joints - by the more prominent two patterns developed in this region.

The grout holes were executed through the overburden (0.0-3.0m) and decomposed / very highly weathered rock by rotary drilling - diameter 101mm (Rig : Wirth BO/B1A) with casing diameter 86mm. There onwards till the final depth - 24m drilling was performed by percussion (Track drill rig : Atlas Copco) method. These holes were with a diameter of 64mm and an inclination of 20° (from vertical) directed towards North.

According to the test programme (Fig. 6) the testing was to be carried out in four consecutive phases each phase followed by a check hole drilled by rotary method with core recovery in the centre of the triangle in which water

pressure tests (Lugeon type) are conducted to check the effectiveness of grouting.

Also with the obtained core, the effectiveness of grouting could be checked by inspecting the grouted joints. As shown on Fig. 7, after phase I, the pressure tests done, in test hole I (TH I) indicated absorptions (below excavation limits) less than 5 Lugeons, the rock is considered as technically (nominally) impervious which means sufficiently grouted i.e. further grouting not required.

Also after phase II grouting, test hole II (TH II) confirmed the same. Phase III was simply carried out to obtain additional information though in reality the whole test programme could be stopped after Phase II. On the basis of above data it could be concluded that for the highly to very highly permeable foundations of Dam, a 3m spacing in any direction between holes (means between grout fans too) can be effectively used. Here also it should be pointed out as shown on the Engineering Geological map of the core trench it was apparent that the most parts of the foundation are similar to the test area in intensity of jointing. Please see Fig. 1 - Engineering Geological map of the core trench.

Test Grouting Programme II: For the lower section (curtain below the grouting gallery) of the grout curtain.

The test area in which this test was carried out approximately corresponds to chainage D₂+330 and D₂+340 of the core trench (Fig. 5). At depths from 0.00 to 14.00m no testing was performed as consolidation grouting in this reach is to be done and as the deep grout curtain in the Dam foundation will be always executed in rock moderately weathered or fresh and these types of rock always occur below about 15m.

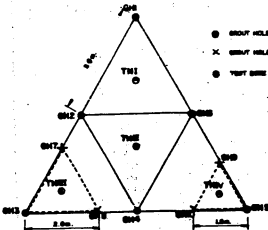
Drilling and grouting was performed in two consecutive phases (I & II) as shown on Fig. 7. All grout holes No. GH1 to GH7 were drilled with percussion method directed towards North, inclined 20° and were grouted in descending 3m stages - in the upper sections where intakes have been high, and in 6m stages - where intakes have been low. Water pressure testing always followed grouting where an intake has been recorded by the pressure test, performed before grouting. If the second water pressure test indicated absorption more than 5 Lugeons after initial grouting - a secondary grouting was done till refusal.

After completing grouting of Phase I and II, two test holes (TH IV and TH V) were drilled by rotary method inclined and directed towards South in order to pierce through the zone already grouted.

In grout holes (Nos. 1,2,3,4,5,6 & 7) and in both test holes (TH IV and V) inclinometry measurements were performed to establish the deviations of the actual hole from the designed theoretical one. Results of these measurements (horizontal & vertical projections) are given in Figs. 8 and 9.

TEST EXECUTION PROGRAMME

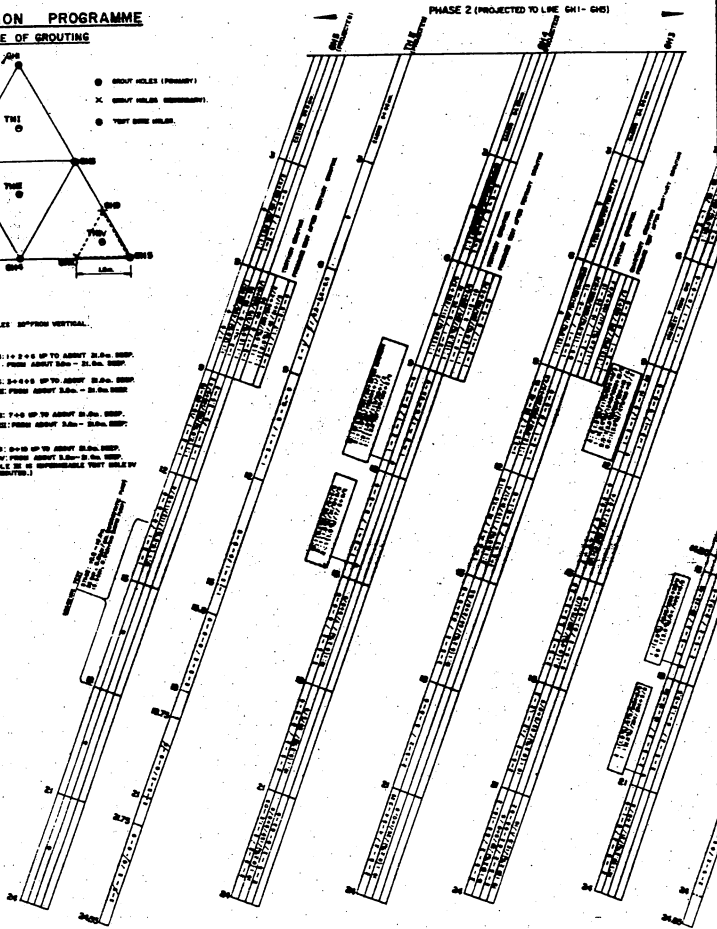
TRIANGLE OF GROUTING

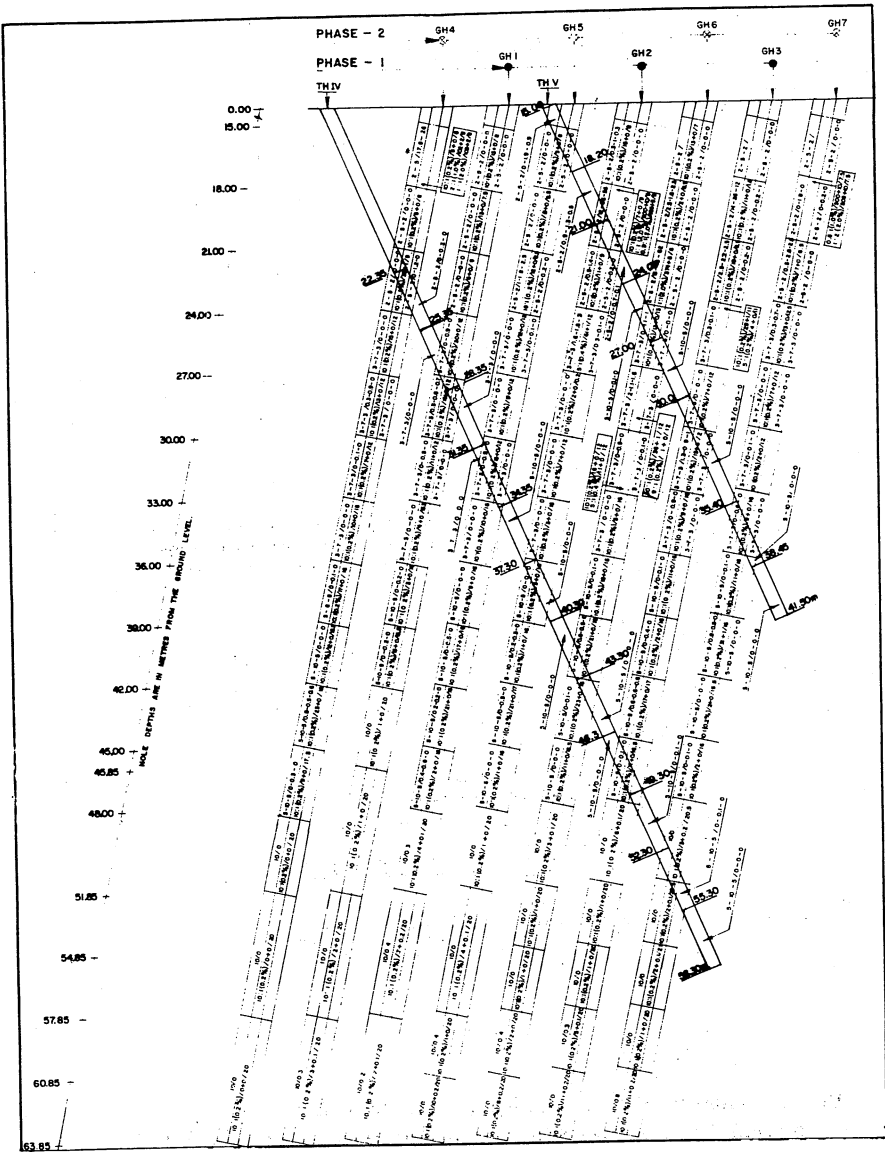


NOTES:

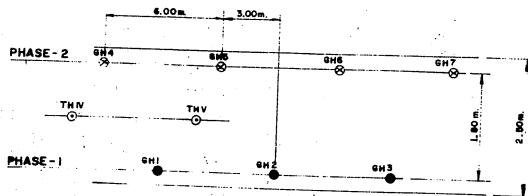
SPACERS = 4.5m.
 INCLINATION OF ALL HOLES 50° FROM VERTICAL.
 DIRECTION = 0° OF 2°

- PHASE 1: GROUT HOLES: 1-0-0-0 UP TO ABOUT 2.5m DEEP.
 TEST HOLES: FROM ABOUT 2.5m - 2.5m DEEP.
- PHASE 2: GROUT HOLES: 2-0-0-0 UP TO ABOUT 2.5m DEEP.
 TEST HOLES: FROM ABOUT 2.5m - 2.5m DEEP.
- PHASE 3: GROUT HOLES: 3-0-0-0 UP TO ABOUT 2.5m DEEP.
 TEST HOLES: FROM ABOUT 2.5m - 2.5m DEEP.
- PHASE 4: GROUT HOLES: 0-0-0-0 UP TO ABOUT 2.5m DEEP.
 TEST HOLES: FROM ABOUT 2.5m - 2.5m DEEP.
 (ALL TEST HOLES TO BE RESPONSIBLY TEST HOLES BY THE TEST CONTRACTOR.)





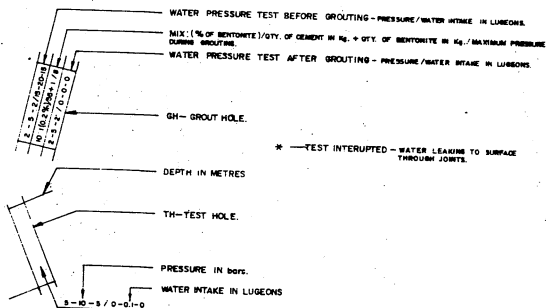
SPACING AND PHASES OF GROUT HOLES - PLAN



GROUT HOLES

- PHASE-1 GH1, GH2, GH3 — 63.0m. DEEP.
- PHASE-2 GH4, GH5, GH6, GH7 — 63.0m. DEEP.
- TEST HOLES

LEGEND:-



NOTES:-

1. GROUT HOLES OF PHASE-3 WERE NOT EXECUTED AS THE TEST HOLES 1 AND 2 EXECUTED AFTER GROUTING PHASE 1 AND 2, WERE FOUND TIGHT.
2. ALL GROUT HOLES (GH) AS WELL AS TEST HOLES (TH) WERE DRILLED FROM THE NATURAL GROUND SURFACE THROUGH THE OVERBURDEN (APPROXIMATELY 15 CM THICK.) GROUTING TESTS WERE STARTED FROM A DEPTH OF ABOUT 15.0m FROM THE SURFACE I.E. ROCK.

**Fig. 7.- Results of Test Grouting - Program II
Performed for the Lower Section of the Deep Grout Curtain**

For all grouting works the water cement mixes were prepared and used as shown in the Table No.2.

TABLE 2.- Water Cement Mixes for Grouting Works

Water absorption test in Lugeons	Cement Ratio	Admixture (in %) Bentonite
1 - 3	1:10 to 1:6	2
3 - 6	1:5 to 1:3	2
6 - 12	1:2	3
12 - 20	1:1	3
>20	1:0.9 to 1:0.5	3

TABLE 3.- The pressures to be used for water pressure tests depending on the depth

Depth in metres		Pressure bars
From	To	
15.00	- 24.00	2 - 5 - 2
24.00	- 36.00	3 - 7 - 3
36.00	- 48.00	5 - 10 - 5
48.00	- 64.00	10 (water pressure tested only with one pressure)

According to the data obtained from the above tests the following conclusions were arrived at :

- As some holes grouted in Phase II and both test holes were found tight the curtain grouting should be performed in the same sequence and with the same spacing between grout holes. The grouting procedure too is satisfactory and therefore can be adopted for construction of the curtain as well.

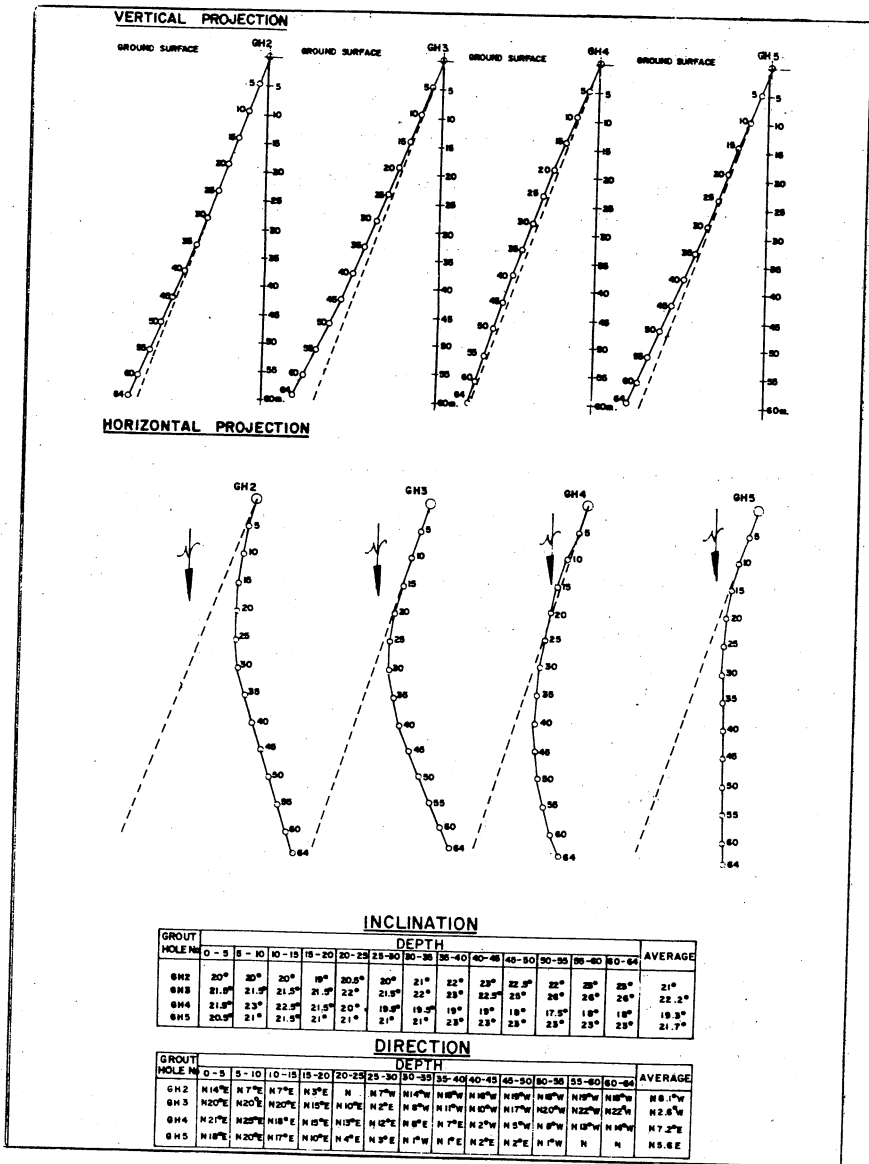
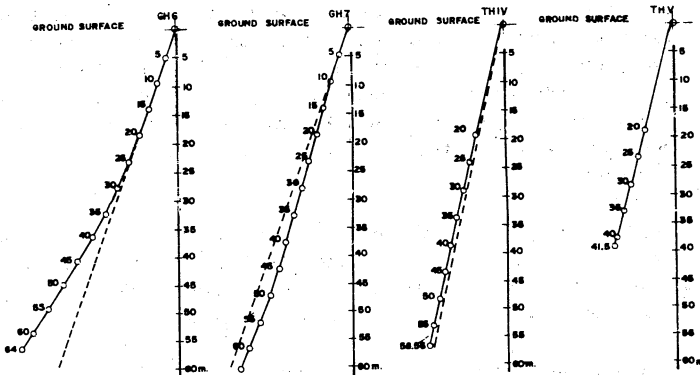
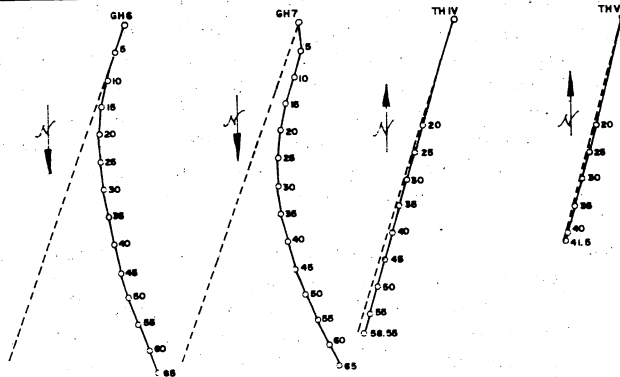


Fig. 8.- Results of Test Grouting - Program II
Inclinometry

VERTICAL PROJECTION



HORIZONTAL PROJECTION



INCLINATION

GROUP	DEPTH															AVERAGE
	HOLE	0-5	5-10	10-15	15-20	20-25	25-30	30-35	35-40	40-45	45-50	50-55	55-60	60-65		
GH6	20°	20°	18.5°	18°	21°	24°	26°	27°	30°	31°	31.5°	32°	32.5°	24.9°		
GH7	20°	19°	16°	16°	15°	15.5°	15°	16°	16°	17°	20°	21°	18.7°	18.7°		
THIV	15°	15°	13°	13°	13°	13°	13°	13°	13°	13°	13°	13°	13°	13°		
THV	15°	15°	15°	15°	15°	15°	15°	15°	15°	15°	15°	15°	15°	15°		

DIRECTION

GROUP	DEPTH															AVERAGE
	HOLE	0-5	5-10	10-15	15-20	20-25	25-30	30-35	35-40	40-45	45-50	50-55	55-60	60-65		
GH6	N20°E	N17°E	N11°E	N6°E	N2°W	N6°W	N8°W	N12°W	N12°W	N8°W	N8°W	N22°W	N22°W	N7.3°W		
GH7	N3°W	N5°E	N20°E	N10°E	N5°E	N1°E	N3°W	N12°W	N14°W	N20°W	N23°W	N25°W	N25°W	N6.7°W		
THIV	S18°W	S18°W	S18°W	S18°W	S18°W	S18°W	S18°W	S18°W	S18°W	S18°W	S18°W	S18°W	S18°W	S18°W		
THV	S18°W	S18°W	S18°W	S18°W	S17°W	S17.5°W	S17°W	S17°W	S17°W	S17°W	S17°W	S17°W	S17°W	S16.8°W		

**Fig. 9.- Results of Test Grouting - Program II
Inclinometry**

- Deviations (from the designed) of grout holes (as shown on Fig. 8 & 9) drilled by percussion method were reaching unacceptable limits (accepted limit was a deviation from the theoretical position up to 3% of the length of hole) for depths exceeding about +20m. Hence for drilling grout holes more than 20m deep percussion method can not be used, but rotary method (as indicated by the inclinometry measurements in test holes TH IV and V) can be utilised successfully.

Therefore, all grout holes (above the grouting gallery for consolidation) of the upper section of the grout curtain will be executed by percussion method whereas the grout holes (below the grouting gallery) of the lower section of the curtain will be executed by rotary method.

Conclusions and Recommendations for Execution

Prior to execution of the grout curtain the entire rock mass to a depth of 4m around the grouting gallery should be consolidated by injecting cement grout. The drilling for consolidation grouting shall be by percussion method with 7 Nos. of holes located on a ring (spacing between two holes ± 1.3 m) and the rings are to be 3m apart from each other. The holes shall be located on rings, in a staggered pattern to enhance the effect of grouting. The mixes to be used are of 2:1 and 1:1 water cement-ratios with 2% bentonite. The maximum pressure to be utilised at refusal is 8 bars.

Upper section of the Grout Curtain - above the Grouting Gallery :- This part of the grout curtain should be constructed in a form of a "fan" consisting of six grout holes drilled by percussion method as shown on Fig. 10. These fans would be perpendicular to the Dam axis and at a spacing of 3m from each other. Initially the outer four holes (on line No. 1, 2, 5 & 6) should be drilled and grouted from the core trench. Subsequently, line No. 3 and No. 4 - the centre holes located on a plane between the two consecutive planes in which the outer 4 holes are located, should be executed from the grouting gallery. Out of these two lines No. 3 should be executed first and according to water pressure test results if absorption is found to be more than 5 Lugeons in them, in any location, then the corresponding holes on line No. 4 are to be executed, otherwise not required.

The water pressure tests should be executed in 3m stages under one (maximum) pressure corresponding to the hydrostatic head to be expected in that location when reservoir is impounded, (see Table 3). Same pressure shall be used for grouting as well. The grouting is to be done in ascending or descending method in stages of 3m or 6m depending on the water intakes (water pressure tests). Grouting pressures to be used are from 7 to 14 bars increasing with depth. The mixes are to be used, depending on the intake, as per values given in Table No. 2.

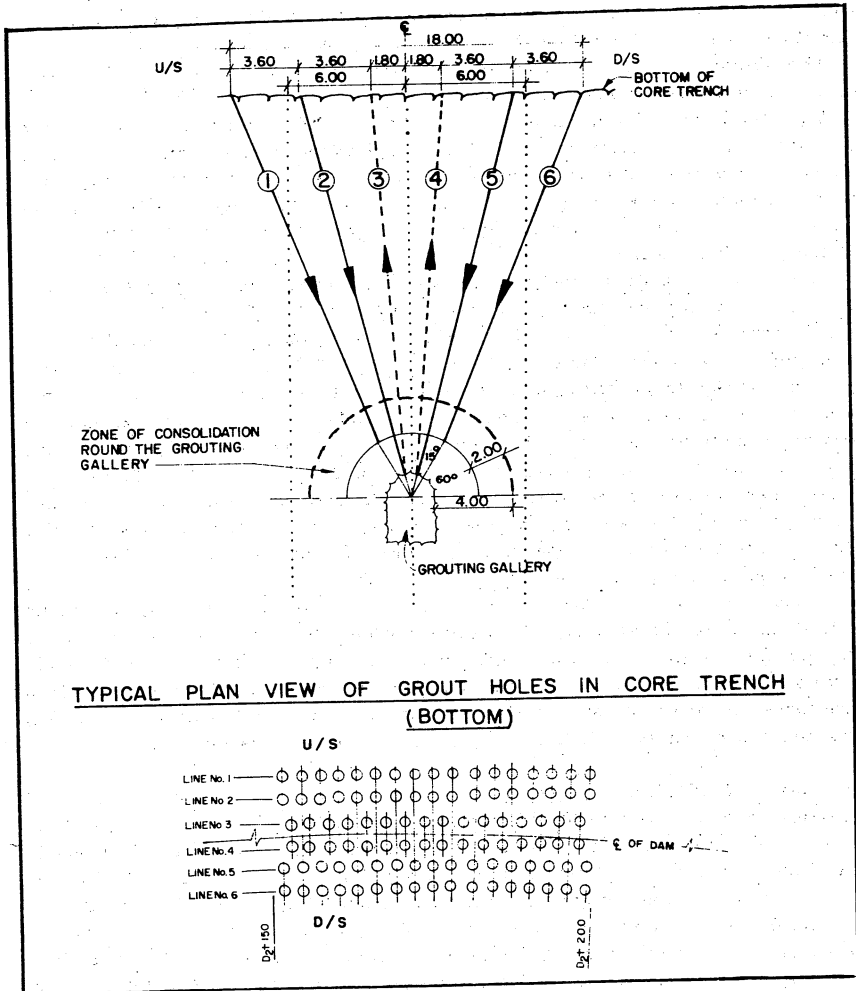


Fig. 10.- Typical Cross Section of the Upper Section of Deep Grout Curtain

Lower Section of the Grout Curtain - Below the Grouting Gallery :- Drilling for the above curtain shall be done from the grouting gallery by rotary method only and the holes should be with an inclination of 22° directed towards Left bank (almost North) with an exception on the Right abutment below Spillway structure where the holes are directed towards almost South.

The above exception is necessary to preserve continuity of the grout curtain and to make execution possible.

The depth of drilling shall be controlled by the criterion of reaching a six metre (two 3m sections) technically impervious (absorption less than 5 Lugeons) zone below 20m from the grouting gallery i.e. depth of drilling shall be suspended when water pressure tests indicate a six metre section without intake or an intake less than 5 Lugeons at a depth below 20m from the invert of the grouting gallery.

Initially, a set of primary holes shall be executed with a six metre spacing on a line parallel to the centre line of the grouting gallery about 50cm upstream of the downstream wall of the gallery. After completion of grouting of the primary holes on the basis of results of water pressure tests conducted prior to grouting, in areas where water intake has been more than 5 Lugeons, a secondary line of grout holes parallel to the primary zones, but located in between them, on a line about 1.5m upstream of the line of primary holes, to the same depth as primary holes shall be executed. Further, in areas where intake of secondary holes are found to be more than 5 Lugeons, after completing the grouting of the secondary holes a tertiary set of holes shall be executed on a line between the lines of primary and secondary holes finally making the grout hole spacing to be 1.5m.

Grouting of all holes shall be with mixes according to Table 2 by ascending method in 3m or 6m stages. The maximum grout pressures (at refusal) to be utilised are from 2.5 to 18 bars depending on the hydrostatic head which would develop at that particular elevation when reservoir is impounded. (low pressures are to be utilised on the abutments). Ascending method of grouting was adopted to minimise drilling length for economical reasons.

Control of Efficiency of Grouting: To check and control the efficiency of grouting, control holes (with NX diameter) shall be drilled from the grouting gallery with core recovery in areas where intakes of more than 5 Lugeons in the upper section as well as in lower section of the grout curtain. For the upper section these holes can be directed either towards LB or RB upwards with an inclination of about 45° from vertical. For the lower section control holes shall be directed in the opposite direction of the grout holes i.e. towards RB generally (on the edge of the right abutment towards LB) with an inclination of about 45° . In these holes pressure tests shall be carried out with pressures corresponding to those used for grouting in these locations.

Normally the control holes should be without any intake but in any case if found to be having absorptions higher than 5 Lugeons, they shall be grouted

with the procedures adopted for initial grouting.

The obtained core samples shall be inspected for grout in joints and shall be preserved for future use.

Acknowledgement

The author wishes to express his gratitude to Mr.S.Dantanarayana who prepared the illustrations and Mrs. G.H. Manel who typed the manuscript.

Appendix I- References

1. Bulletin of the International Association of Engineering Geology No.24, 1981.
2. Cooray P.G. An Introduction to the Geology of Ceylon, National Museums of Ceylon Publication 1967.
3. Ewert F.K. Rock grouting with Emphasis on Dam Sites. Springer-Verlag - Heidelberg 1985.
4. Irapetian R.A. Design of Rock Fill Dams. Energy Publications - Moscow 1968.
5. Report on Engineering Geology of Randenigala Project - Salzgitter Consult GmbH, Salzgitter, FRG, March 1981.
6. Sherard J.L. et al, Earth and Earth-Rock Dams, John Wiley & Sons. Inc. new York 1977.

UNDRAINED BEHAVIOR OF K_0 CONSOLIDATED CLAYS AT FAILURE.

By Thevanayagam. S¹

ABSTRACT: Recent advances in fundamental basis of Cam Clay Models are summarized. A general ultimate failure criterion is introduced. Based on these, a simple method to predict undrained shear strength, angle of friction and pore pressure at failure for K_0 consolidated clays is presented. The model takes into account many experimentally observed anisotropic features of natural clays. Given the friction angle, ϕ_c , from a triaxial compression test and over consolidation ratio (OCR) of the clay, the model can predict undrained shear strength, friction angle, and pore pressure at failure for many conventional stress paths such as in plane strain compression/extension, simple shear and triaxial extension tests. In addition, the model allows to transform the failure parameters obtained from any one of the above tests to predict undrained shear strength for any other stress path. The model capability is demonstrated using experimental data for clays of many geologic origin and over consolidation history.

Introduction

Experimental studies conducted in the past have elucidated the significance of anisotropy on the shear behavior of natural clays (Duncan and Seed 1966, Lewin 1973, Mitchell 1972, Saada and Bianchini 1975, Tavenas and Leroueil 1977, Ting 1968). Lewin's stress probe experiments showed differences between lateral and axial strains during isotropic consolidation of an initially anisotropic specimen of clay. Anisotropy can also be induced; Ting (1968) showed that an anisotropically consolidated sample reaches an asymptotic isotropic state at an isotropic stress about 3 times higher than its initial vertical stress. Available experimental data (e.g., Tavenas and Leroueil 1977, Graham et al. 1983) show that the yield loci of natural clay deposits are centered around K_0 line in triaxial p-q stress space. These facts of anisotropy must be included by geotechnical engineers if major improvements in their design of earth structures are to be created.

Many methods have been proposed to obtain the undrained strength of in-situ clays along a few stress paths (e.g., Ladd et.al., 1974; Prevost, 1979; Wroth, 1984; and Maine, 1985 among others). Some (e.g. Wroth, 1984) are based on an isotropic soil model even though evidence exists that the natural clays

¹Staff Engineer, Earth Technology Corporation, 100 West Broadway, Suit 5000, Long Beach, CA 90802, USA.

are anisotropic. Ladd et. al. (1974) proposed an experimental procedure (SHANSEP) that requires reconsolidation of "undisturbed" samples to the initial K_0 state and extensive testing, which can be very expensive, and provides only point estimates along the specific stress paths of tests. Some models (e.g., Prevost 1979) are based on the assumption that the mean stress at failure is independent of the mode of failure, and are therefore not general. In addition K_0 consolidated triaxial tests are required to calibrate these models.

A simple model shall capture the important aspects of anisotropy and offer closed form solutions for strength (and other soil parameters at failure) along various distinct stress paths, as, for example along a slip surface at various orientations through the mass in an embankment or a slope. Such a model will be very valuable to the designer.

The purpose of this work is to create a simple plasticity model that captures the behavior of clays at the critical state. The emphasis for this model is upon: i) the anisotropic nature of the yield surface, ii) the effect of induced anisotropy, iii) predicting failure parameters of clays, using simple parameters (friction angle ϕ_c obtained from an isotropically consolidated triaxial compression test (CIUC) and overconsolidation ratio, (OCR), and iv) the ability to interpret any measured insitu strength, and transform it to any other stress path applicable for a given design problem. Test results published in the literature have been used to verify the model. These include many natural soils that have been tested in triaxial compression/extension (TC/TE), plane strain compression/extension (PSC/PSE), and simple shear (SS). The use of this model can reduce the amount and cost of testing, and can also enlarge the range of design analyses that can be performed because appropriate soil strength parameters can now be made readily available.

The notations in this paper (Appendix II) are that of critical state soil mechanics (Schofield and wroth 1968). All stresses in the text and equations are effective stresses. Natural clays are, due to their mode of deposition, generally cross anisotropy; the vertical axis is assumed to be the axis of cross anisotropy. For simplicity, elastic properties are assumed to be isotropic.

Cam Clay Models

The pioneering work of Roscoe, Schofield and Thurairajah (1963) lead to the development of Cam Clay models. The original Cam Clay theory was based on the following work assumption:

$$p \dot{\epsilon}_y + q \dot{\epsilon}_q = M p \dot{\epsilon}_q \quad (1)$$

Considering the continuity requirements of work relation, Eq.1, it was modified to the form (the Modified Cam Clay model (M.C.C)) (Rescoe and Burland, 1968), as given by

$$p \dot{\epsilon}_V^D + q \dot{\epsilon}_q^D = p \left[(\dot{\epsilon}_V^D)^2 + (M \dot{\epsilon}_q^D)^2 \right]^{1/2} \quad (2)$$

which, assuming the associative flow rule, resulted in the isotropic yield surface of the form:

$$f_{ISO} = p^2 - p p_0 + \frac{q^2}{M^2} = 0 \quad (3)$$

Dafalias (1987) introduced the following modification of the work assumption.

$$p \dot{\epsilon}_V^D + q \dot{\epsilon}_q^D = p \left[(\dot{\epsilon}_V^D)^2 + (M \dot{\epsilon}_q^D)^2 + 2 \alpha \dot{\epsilon}_V^D \dot{\epsilon}_q^D \right]^{1/2} \quad (4a)$$

where α is a nondimensional parameter with an absolute value less than M. The term α is considered to account for anisotropic internal residual stresses in the clay.

In general these work assumptions can be described in the form of a strain-dilatancy relationship given by ;

$$\frac{\dot{\epsilon}_V^D}{\dot{\epsilon}_q^D} = \frac{M^2 - \eta^2}{2(\eta - \alpha)} \quad (4b)$$

This implies that the plastic response of the soil is controlled by the relative position of the current state of stress (η) with respect to two reference states, the critical state at $\eta = M$ and another state where $\eta = \alpha$. As the state of stress becomes closer to the critical state the tendency for plastic compaction ($\dot{\epsilon}_V^D$) gradually decreases. As η tends closer to α , the plastic compaction increases whereas the plastic slip ($\dot{\epsilon}_q^D$) decreases. The two reference states ($\eta = M$ and $\eta = \alpha$) refer to two states of fabric where $\dot{\epsilon}_V^D = 0$ and $\dot{\epsilon}_q^D = 0$ under any induced loading conditions respectively. Hence, α could be related more closely to fabric of soils. For an isotropic state of fabric α becomes zero. Since fabric could be altered during shear, α could vary with shearing.

Hence, the selection of the reference parameter α dictates the importance of the coupling term in Eq.4a or 4b. Thus, in general, α must be a function of state parameters of a clay. The assumption $\alpha = 0$ (Roscoe and Burland 1968) (compare Eqs. 2 and 4a-b) is obviously a special case of the more general formulation using Eq. 4a or 4b. If a non-zero constant value (to account for anisotropy) is assumed, it is appropriate to relate it to the state at the end of K_0 virgin consolidation of the clay from a slurry. During K_0 virgin consolidation, the following conditions must be satisfied.

$$\frac{\dot{\epsilon}_v}{\dot{\epsilon}_p} = 3/2; \quad \frac{\dot{\epsilon}_v^p}{\dot{\epsilon}_q^p} = \frac{\dot{\epsilon}_v^e - \dot{\epsilon}_v^e}{\dot{\epsilon}_q^e - \dot{\epsilon}_q^e}; \quad \text{and } \eta_0 = \frac{\dot{q}}{p} = \frac{3(1 - K_0)}{(1 + 2K_0)} \quad (5)$$

where η refers to the slope of the virgin K_0 line in p - q plane. Assuming elastic isotropy and linear e vs. $\ln(p)$ relationships:

$$K = \frac{\dot{p}}{\dot{\epsilon}_v} = \frac{(1 + e)p}{\kappa}; \quad \dot{\epsilon}_q^e = \dot{q} / (3G), \quad \frac{G}{K} = \frac{3(1 - 2\nu)}{2(1 + \nu)} \quad (6)$$

where $K, G,$ and ν are the Elastic Bulk modulus, Shear modulus and Poisson's ratio of the clay, respectively. Denoting the value of α at the end of K_0 virgin consolidation by α_0 , and using Eqs. 5-6, we have

$$\alpha_0 = \frac{3a_1 \eta_0 + \eta_0^2 - M_c^2}{3a_1}; \quad a_1 = \frac{(1 - \kappa/\lambda)}{[\kappa \eta_0 (1 + \nu)] / [3\lambda (1 - 2\nu)]} \quad (7)$$

If the elastic shear strain is neglected in Eq. 5, $a_1 = 1 - \kappa/\lambda$, and α_0 reduces to:

$$\alpha_0 = \frac{3(1 - \kappa/\lambda)\eta_0 + \eta_0^2 - M_c^2}{3(1 - \kappa/\lambda)} \quad (8)$$

If the clay is isotropically consolidated ($\eta_0 = 0, \dot{\epsilon}_q = \dot{\epsilon}_q^p = 0$), α_0 becomes zero.

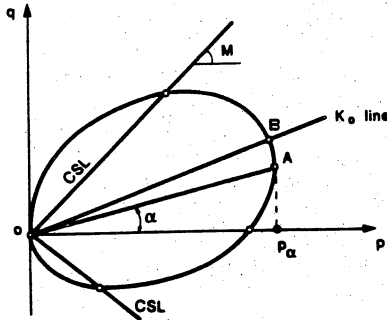


Fig. 1a.- A Typical Yield Surface in the Triaxial p - q space

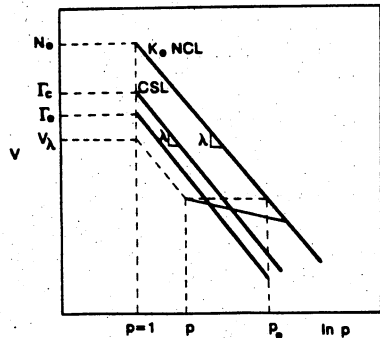


Fig. 1b.- Critical State Parameters

It may be noted that neither an assumption on the shape of yield surface nor the use of flow rules are necessary to derive α_0 .

If associative flow rule and a constant value of α such as $\alpha = \alpha_0$, are assumed, the shape of the yield locus function is deduced from Eq. 4a or 4b as:

$$\frac{p}{p_i} = \frac{M^2 + \eta_i^2 - 2\alpha \eta_i}{M^2 + \eta^2 - 2\alpha \eta} \quad (9)$$

where (p, η) and (p_i, η_i) correspond to any positions on the yield surface, $f=0$ (Fig. 1). M takes the value M_c (corresponding to critical state in triaxial compression) for points located above Point A in Fig. 1 and M_e (extension side) for points below A. The point A corresponds to the condition where $\eta = \alpha$. If α is assumed to remain constant during subsequent loading, then the equations for the state boundary surface are given by:

$$(\eta - \alpha)^2 = - (M^2 - \alpha^2) + \frac{(M^2 - \alpha^2)}{(M_c^2 - \alpha^2)} \left[(\eta_0 - \alpha)^2 + (M_c^2 - \alpha^2) \right] \exp \left[\frac{N_0 - v\lambda}{\lambda - k} \right] \quad (10a)$$

$$\left(\frac{q}{P_e} - \frac{\alpha p}{P_e} \right)^2 = - (M^2 - \alpha^2) \left[\frac{p}{P_e} \right]^2 + \frac{(M^2 - \alpha^2)}{(M_c^2 - \alpha^2)} \left[(\eta_0 - \alpha)^2 + (M_c^2 - \alpha^2) \right] \left[\frac{p}{P_e} \right]^{\frac{\lambda - 2k}{\lambda - k}} \quad (10b)$$

where $M = M_c$, for $\eta \geq \alpha$, and $M = M_e$ for $\eta \leq \alpha$. The parameters P_e , N_0 , and $v\lambda$, are defined as shown in Fig. 1. The state boundary surfaces Eqs. 10a and 10b are plotted in Fig. 2 and 3 (solid lines) for Kaolin using the following parameters: $N_0 = 3.23$, $\lambda = 0.19$, $k = 0.06$, $M_c = 0.85$, and $M_e = -0.85$. The state boundary surfaces predicted from these equations are compared in Fig. 2 and 3 with experimental data on stress paths obtained by Atkinson et. al. (1987). This comparison shows that the model with a constant, α , captures the main features of the state boundary surface with some deviations. The first deviation that occurs in the initial part of TE stress path is however, not completely unexpected. At least the initial part, since it remains inside the yield locus, is expected to be elastic (Thevanayagam and Prapaharan 1989). Therefore, this initial part of the TE stress path is expected to lie inside the state boundary surface. The stress path in TC closely follows the state boundary surface up to the peak deviatoric stress (Fig. 2) and deviates beyond this point. These deviations at large strains may be attributed to the effects of induced anisotropy. If the post peak behavior in TC and large strain behavior in TE are of interest then the induced anisotropy should be accounted for in the model. This means that the model should account for variation of α during shearing.

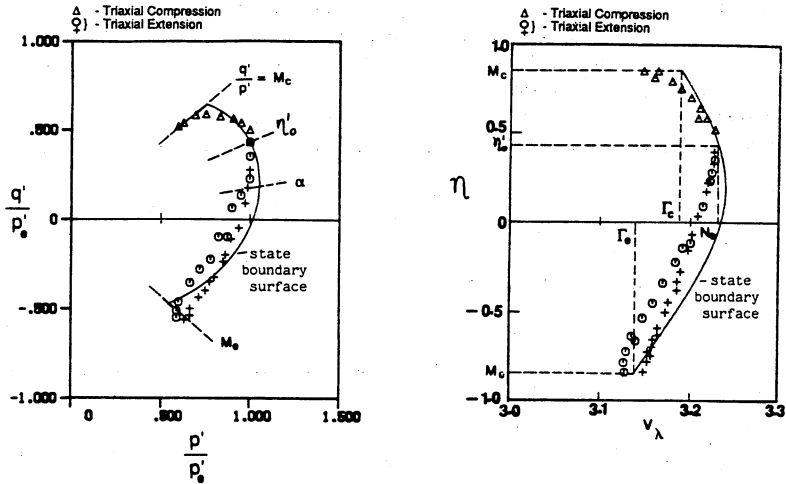


Fig. 2 & 3.- Normalized Stress Paths in TC/TE and State Boundary Surface

In what follows, the effects of induced anisotropy are introduced by considering that α does not remain constant, but varies during shearing proportionally to the initial value of α_0 , i.e., $\alpha = \gamma \alpha_0$. The other assumptions of the model related to other evolution characteristics of the yield surface f are: (i) the projection of the yield surface onto the e vs. $\ln(p)$ plane has a constant slope k , and (ii) the hardening is such that the point E in Fig. 1 projected onto the e vs. $\ln(p)$ plane remains on the K_0 NC line independent of the plastic loading.

The expressions for peak undrained strength ratio (τ_f / σ_{v0}) (where σ_{v0} is the initial vertical effective stress and τ_f is the peak undrained shear strength) in TC and TE are developed first. The value of γ in TC and TE are obtained by calibrating the theoretical expressions, for strength ratio using experimental data.

Undrained shear in Triaxial Compression: Using the equation for the yield surface, the undrained strength in TC is given by:

$$\left(\frac{\tau_f}{\sigma_{v0}}\right)_{OC} = \left(\frac{\tau_f}{\sigma_{v0}}\right)_{nc} \left[\frac{1+2K_{0,OC}}{1+2K_{0,nc}} \right]^{\frac{k}{\lambda}} \left[OCR \right]^{\Lambda}; \quad \Lambda = 1 - \frac{k}{\lambda} \quad (11)$$

where

$$\left(\frac{\tau_f}{\sigma_{v0}}\right)_{nc} = \frac{(1+2K_{0,nc})M_c}{6} \left[\frac{M_c^2 + \eta_0^2 - 2\alpha\eta_0}{2M_c^2 - 2\alpha M_c} \right]^{\Lambda}$$

α represents the anisotropic state at failure and nc and oc stand for normally consolidated clay and overconsolidated clay, respectively. If α is set to zero, Eq. 11 reduces to the strength expressions for CK_{OC} strength and $CIUC$ (when $\eta_0=0$, and $K_0=1$) strength using the MCC model (Wroth 1984). Equation 11 can be further simplified as follows.

The slopes of swelling and virgin consolidation lines k and λ obtained from e vs. $\ln(p)$ plane, and k_v and λ_v obtained from e vs. $\ln(\sigma_v)$ plane can be related by:

$$\lambda = \lambda_v \text{ and } k = \left[\frac{\ln(OCR)}{\ln \left[\frac{(1+2K_{0,nc})OCR}{(1+2K_{0,oc})} \right]} \right] k_v \quad (12)$$

for any OCR. Using typical K_0 -OCR relationships (e.g., Brooker and Ireland 1965) the value of k can be simplified as $k=1.3 k_v$ and Eq. 11 reduces to:

$$\left(\frac{\tau_f}{\sigma_{v0}} \right)_{oc} = \left(\frac{\tau_f}{\sigma_{v0}} \right)_{nc} (OCR)^{\lambda_v}, \quad \lambda_v = 1 - \frac{k_v}{\lambda} \quad (13)*$$

It is interesting to note that this general equation does encompass relationships proposed in earlier studies. Equation 13 is similar to the empirical relationship proposed by Ladd, et. al (1977) and the theoretical relationship for isotropic clays (Wroth 1984).

Undrained Shear in Triaxial Extension: Similarly, the undrained shear strength in TE is given by:

$$\left(\frac{\tau_f}{\sigma_{v0}} \right)_{TE} = \frac{M_e}{M_c} \cdot \frac{M_e^2 - \alpha^2}{M_c^2 - \alpha^2} \left(\frac{\tau_f}{\sigma_{v0}} \right)_{TC} \left[\frac{M_c(M_c - \alpha)}{(M_e + \alpha)M_e} \right] \left(1 - \frac{1.3k_v}{\lambda} \right) \quad (14)$$

where $(\tau_f / \sigma_{v0})_{TC}$ is given by Eq. 11 or 13; α represents the degree of anisotropy at the critical state after shearing in TE in this case. Note that the value of M_e is negative. Classically, critical state parameters M_c and M_e are obtained using the Mohr-Coulomb criteria (Roscoe and Burland 1968, Dafalias 1987) as: $M_c = 6 \sin \phi / (3 - \sin \phi)$ and $M_e = -6 \sin \phi / (3 + \sin \phi)$, where ϕ is the angle of friction at failure obtained from TC ($\sin \phi = (\sigma_1 - \sigma_3) / (\sigma_1 + \sigma_3)$ at $(\sigma_1 - \sigma_3)_{max}$). However, these expressions are valid only for truly isotropic clays. Existing data (e.g., Saada and Bianchini, 1975) show that for 1-D consolidated clays the friction angle, ϕ_e , in TE is generally greater than that, ϕ_c , in TC. In this work, using the failure criteria developed later in Eq. 21, a different relationship was obtained for friction

* Susequently left hand side of Eq. 13 is written as $(\tau_f / \sigma_{v0})_{TC}$ in general

angles ϕ_c in TC and ϕ_e in TE (demonstrated in Eq. 21 and comparison with data showed very good agreement (see Fig. 5 introduced later in this paper)). Using this information, Eq. 14 can be reduced to a simple expression (absolute value of τ_f in TE is taken):

$$\left(\frac{\tau_f}{\sigma_{v0}}\right)_{TE} = \left[\frac{M_c - \alpha}{M_c + \alpha} \right] \left(1 - \frac{1.3k_v}{\lambda}\right) \left(\frac{\tau_f}{\sigma_{v0}}\right)_{TC} \quad (15)$$

Further simplifications can even be made if desired. Using a typical value of $k_v/\lambda = 0.2$, taking a Taylor series expansion, and neglecting higher order terms Eq. 15 reduces to:

$$\left(\frac{\tau_f}{\sigma_{v0}}\right)_{TE} = \left(\frac{M_c - 0.5\alpha}{M_c + \alpha}\right) \left(\frac{\tau_f}{\sigma_{v0}}\right)_{TC} \quad (16)$$

Induced Anisotropy and Variation in Soil Parameters: Using experimental data for the peak strength of many clays (Table 1), the values of the proportionally parameter γ in TC and TE were calibrated, considering the following three cases:

- a. $\alpha = 0$ (i.e., isotropic MCC model);
- b. Initial value of α , α_0 , given by Eq. 8; at critical state α is given by $\alpha = \gamma \alpha_0$;
- c. Case (b), but using Eq. 7 for α_0 .

Case (a) when compared to cases (b) and (c) is used to study whether the initial anisotropy is an important factor in the undrained strength ratio of clays. Cases (b) and (c) were chosen to study the influence of Poisson's ratio on the strength ratio. A variation of the ratio k_v/λ in the range of 0.1-0.3, considered to be reasonable, showed that the above relationships were fairly insensitive to this ratio, and most calibrations were thus made with $k_v/\lambda = 0.20$.

For the TC strength (Eqs. 11-13), case (c) was virtually unaffected by any variation in v , and the results were very similar to that of case (b). A regression analysis (not reported herein) showed that case (b) provided the best match with the experimental data with a value of γ essentially equal to 1.0. The predictability of the residual strength of clays was not studied at this stage; it is expected that $\gamma = 1.0$ will not be a satisfactory assumption if the strength at very large strains is of interest. Also the rate effects were not considered in the process of calibration.

For the TE strength, the influence of induced anisotropy was found to be significant compared to TC, and a value of $\gamma = 0.6$ to be most appropriate for the data evaluated, resulting in Fig. 4. However, since the term (τ/σ) TC in Eq. 11-13 is not very sensitive to α , for a simplicity in expressing the

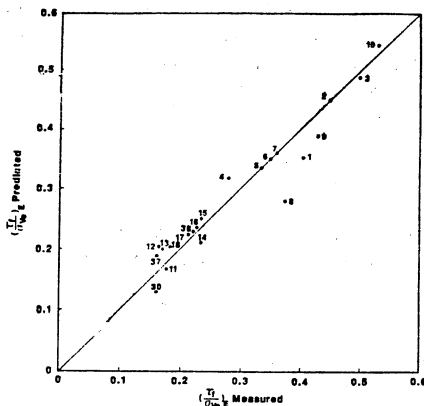


Fig. 4.- Predicted versus Experimental Undrained Strength ratio $\left(\frac{T_f}{\sigma_{vo}}\right)_{TE}$ for Many Clays (Numbers refer to Cases in Table 1)

strength ratio in terms of that in TC, it is sufficient to substitute $\alpha = \gamma \alpha_0$ only in the first term of Eq. 16. For highly overconsolidated clays, since most of the stress path lies inside the yield locus, the induced anisotropy may be expected to be smaller; γ may tend towards 1.0.

3-D Behavior at Critical State

The determination of failure parameters for modes of failure other than TC and TE will now be presented. Let the failure criterion for a clay, given by $f^f = 0$, satisfy the critical state condition, and be dependent on the initial state of the clay. For any arbitrary point A on this failure criterion, the corresponding state of the yield surface is given by f_A . No point can lie outside the failure criterion, and no intersection of yield and failure criteria is possible, except tangentially. Using the associative flow rule, the gradient of f_A at A is perpendicular to the hydrostatic stress axis, as no plastic volumetric strain takes place at critical state. Since f_A and f^f are in contact tangentially at A, the gradient of $f_d = 0$ is parallel to the gradient of f_A at A, where $f_d^f = 0$ is the deviatoric component of the failure criterion, obtained by projecting k^f at a given initial state onto the deviatoric plane in stress space. Since f^f is dependent on the initial state of the clay, the function f_d^f is also dependent on the initial state. The general form of f^f in the 3-D stress space may be obtained by the evolution of the intersection of f_d^f and another, nondeviatoric, surface $f_p^f = 0$. In this development f_p^f is assumed to be independent of the initial state of the clay. The resulting failure surface f^f is given by:

$$f^f = f_d^f + f_p^f = 0 \quad (17)$$

with, $f_d^f = 0$, $f_p^f = 0$ at failure. Using tensor notation the strain increment upon loading at failure (i.e., at critical state) is given by:

$$\dot{\epsilon}_{ij} = \beta \frac{\gamma f_d^f}{\gamma \sigma_{ij}} \quad (18)$$

where β is a proportionality constant. In undrained shearing, only 5 of the 6 components of strain are independent. Therefore, Eq. 18 yields only five independent equations. The functions $f_d^f = 0$, $f_p^f = 0$ offer two more independent equations. The unknowns are the failure stresses (6 components) and the proportionality constant β . Therefore, with the knowledge of the strain increment at failure ϵ_{ij} , and Eqs. 17 and 18, the failure stresses σ_{ij} can be solved for in closed form, (i.e., the strain path and Eqs. 17 and 18 lead to the solution for failure stresses).

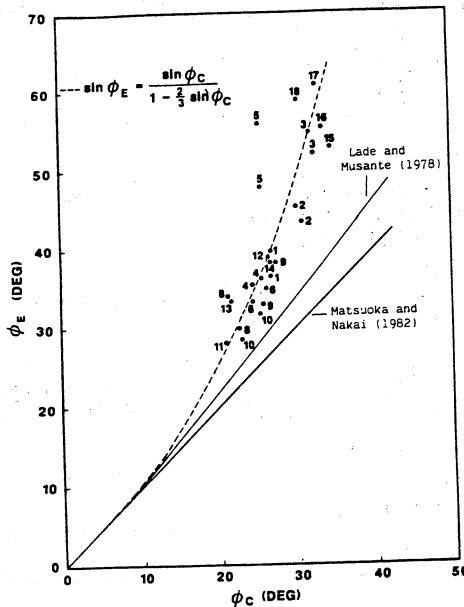


Fig. 5.- Proposed Relationship between ϕ_e and ϕ_c for 1-D Consolidated Clays (Numbers refer to Case in Table 1)

TABLE 1. DATA BANK USED FOR COMPARISON

NOTATION	SOIL	REFERENCE
1 2 3 4 5 6 7 8 9 10	Florida clay - 1 Florida clay - 2 Florida clay - 3 Hydrite - 10-2 Hydrite - 10-3 Girundite - 2 Atchafalay clay - 1 Atchafalay clay - 2 Atchafalay clay - 3 Atchafalay clay - 4	Saada, et al. (1975)
11 12 13 14	Spestone kaolin Boston Blue clay Haney clay Remolded Sapparo	Parry and Nadarajah (1974) Ladd (1965) Vaid, et al. (1974) Mitachi and Kitago (1979)
15 16 17 18	Kawaski - M-30 clay Kawaski - M-20 clay Kawaski - M-15 clay Kawaski - M-10 clay	Nakase and Kamei (1983)
19 20 21 22 23	Weald clay Vicksburg Buck Shot clay Undisturbed Kawaski clay Undisturbed Brobekkvein clay Undisturbed Skabo clay	Ladd (1965)
24 25 26	Hokkaido silt - 1 Hokkaido silt - 2 Hokkaido clay	Mitachi and Kitago (1976)
27 28 29	Boston Blue clay Kaolinite (K100) Kaolinite (k50)	D'Appolonia, et al. (1971) Sivakugan (1987) Sivakugan (1987)
30 31 32 33 34 35 36 37 38	Portsmouth Sensitive Marine clay Bangkok clay San Francisco Bay mud Weald clay Portland Marine clay Marine Organic clay Resedimented BBC Connecticut-Northampton Varved clay Atchafalay clay	Lacasse and Ladd (1973) Ladd and Edgers (1972) Dickey, Ladd and Rixner (1968)

Table 2. Failure Parameters At Critical State of Clays

Failure Mode Parameter	TC	TE	PSC	PSE	S + S	PM
Strain Path	$\dot{\epsilon}_{22} = \dot{\epsilon}_{33} = -\frac{\dot{\epsilon}_{11}}{2}$ $\dot{\epsilon}_{11} > 0$ $\dot{\epsilon}_{ij} = 0 \text{ } i \neq j$	$\dot{\epsilon}_{22} = \dot{\epsilon}_{33} = -\frac{\dot{\epsilon}_{11}}{2}$ $\dot{\epsilon}_{11} < 0$ $\dot{\epsilon}_{ij} = 0 \text{ } i \neq j$	$\dot{\epsilon}_{33} = \dot{\epsilon}_{11}, \dot{\epsilon}_{11} > 0$ $\dot{\epsilon}_{22} = 0$ $\dot{\epsilon}_{ij} = 0 \text{ } i \neq j$	$\dot{\epsilon}_{33} = \dot{\epsilon}_{11}, \dot{\epsilon}_{11} < 0$ $\dot{\epsilon}_{22} = 0$ $\dot{\epsilon}_{ij} = 0 \text{ } i \neq j$	$\dot{\epsilon}_{ij} = 0; i \neq j$ $\dot{\epsilon}_{13} > 0$ $\dot{\epsilon}_{23} = -\dot{\epsilon}_{12} = 0$ $\tau_{13} = \tau_{12}$	$\dot{\epsilon}_{11} = 0$ $\dot{\epsilon}_{22} = -\dot{\epsilon}_{33}$ $\dot{\epsilon}_{ij} = 0 \text{ } i \neq j$
τ_1	$\frac{(\sigma_1 - \sigma_3)_{\max}}{2}$	$\frac{(\sigma_3 - \sigma_1)_{\max}}{2}$	$\frac{(\sigma_1 - \sigma_3)_{\max}}{2}$	$\frac{(\sigma_3 - \sigma_1)_{\max}}{2}$	$(\tau_h)_{\max}$	$\frac{(\sigma_3 - \sigma_1)_{\max}}{2}$
$\frac{(\tau_1)_{YY}}{(\tau_1)_{TC}}$	1.0	$\frac{(M_C - 0.5\alpha)}{(M_C + \alpha)}$	$\frac{(1.15M_C + 1.04\alpha)}{(M_C + \alpha)}$	$\frac{(1.15M_C - 0.46\alpha)}{(M_C + \alpha)}$	$\frac{2M_C + 0.5\alpha}{\sqrt{3}(M_C + \alpha)}$	$\frac{(2M_C + 0.5\alpha)}{\sqrt{3}(M_C + \alpha)}$
$\left(\frac{\sigma_1}{\sigma_{V_0}}\right)_{YY}$	$\left(\frac{4M_C + 6}{3M_C}\right) \cdot \left(\frac{\tau_1}{\sigma_{V_0}}\right)_{TC}$	$\frac{6 - 4M_C}{3M_C}$ $\frac{M_C - 0.5\alpha}{M_C + \alpha} \cdot \left(\frac{\tau_1}{\sigma_{V_0}}\right)_{TC}$	$\left[\frac{X}{M_C\sqrt{2}} + 1.15M_C + 1.29\alpha\right] \cdot \left(\frac{\tau_1}{\sigma_{V_0}}\right)_{TC}$	$\left[\frac{X}{M_C\sqrt{2}} + 0.71\alpha - 1.15M_C\right] \cdot \left(\frac{\tau_1}{\sigma_{V_0}}\right)_{TC}$	--	$\left[\frac{\sqrt{3X^2 + 2.25}}{M_C} - X - 0.5\right] \cdot \left(\frac{\tau_1}{\sigma_{V_0}}\right)_{TC}$
$\left(\frac{\sigma_2}{\sigma_{V_0}}\right)_{YY}$	$\frac{6 - 2M_C}{3M_C} \cdot \left(\frac{\tau_1}{\sigma_{V_0}}\right)_{TC}$	$\frac{6 + 2M_C}{3M_C}$ $\frac{M_C - 0.5\alpha}{M_C + \alpha} \cdot \left(\frac{\tau_1}{\sigma_{V_0}}\right)_{TC}$	$\left[\frac{X}{M_C\sqrt{2}} - 0.5\alpha\right] \cdot \left(\frac{\tau_1}{\sigma_{V_0}}\right)_{TC}$	$\left[\frac{X}{M_C\sqrt{2}} - 0.5\alpha\right] \cdot \left(\frac{\tau_1}{\sigma_{V_0}}\right)_{TC}$	--	$\left[\frac{\sqrt{3X^2 + 2.25}}{M_C} + 1\right] \cdot \left(\frac{\tau_1}{\sigma_{V_0}}\right)_{TC}$
$\left(\frac{\sigma_3}{\sigma_{V_0}}\right)_{YY}$	$\left(\frac{\sigma_2}{\sigma_{V_0}}\right)$	$\left(\frac{\sigma_2}{\sigma_{V_0}}\right)$	$\left[\frac{X}{M_C\sqrt{2}} - 1.15M_C - 0.79\alpha\right] \cdot \left(\frac{\tau_1}{\sigma_{V_0}}\right)_{TC}$	$\left[\frac{X}{M_C\sqrt{2}} - 0.21\alpha - 1.15M_C\right] \cdot \left(\frac{\tau_1}{\sigma_{V_0}}\right)_{TC}$	--	$\left[\frac{\sqrt{3X^2 + 2.25}}{3} - X - 0.5\right] \cdot \left(\frac{\tau_1}{\sigma_{V_0}}\right)_{TC}$
$\sin(\phi_{YY})$	$\frac{3M_C}{6 + M_C}$	$\frac{3M_C}{6 - M_C}$	$\frac{2.31M_C + 2.08\alpha}{\frac{X\sqrt{2}}{M_C} + 1.5 - \alpha}$	$\frac{2.31M_C - 0.92\alpha}{\frac{X\sqrt{2}}{M_C} + 1.5 + \alpha}$	--	$\frac{2M_C X}{2\sqrt{3X^2 + 2.25} - M_C}$
$\frac{\Delta U_{sh}}{(\sigma_{V_0})_{YY}} = \frac{(P_0 - P_1)}{\sigma_{V_0}}$	$\frac{1 + 2K_0}{3} - \frac{2}{M_C} \cdot \left(\frac{\tau_1}{\sigma_{V_0}}\right)_{TC}$	$\frac{1 + 2K_0}{3} - \frac{2}{M_C} \cdot \frac{M_C - 0.5\alpha}{M_C + \alpha}$ $\left(\frac{\tau_1}{\sigma_{V_0}}\right)_{TC}$	$\frac{1 + 2K_0}{3} - \left[\frac{X}{M_C\sqrt{2}} - 1\right] \cdot \left(\frac{\tau_1}{\sigma_{V_0}}\right)_{TC}$	$\frac{1 + 2K_0}{3} - \left[\frac{X}{(M_C + \alpha)M_C\sqrt{2}}\right] \cdot \left(\frac{\tau_1}{\sigma_{V_0}}\right)_{TC}$	--	$\frac{1 + 2K_0}{3} - \frac{2}{\sqrt{3X^2 + 2.25}} \cdot \frac{M_C}{M_C + \alpha} \cdot \left(\frac{\tau_1}{\sigma_{V_0}}\right)_{TC}$
X	--	--	$7.98M_C^2 - 14.35M_C\alpha + 7.61\alpha^2)_{1/2}$	$7.98M_C^2 - 6.35M_C\alpha + 2.39\alpha^2)_{1/2}$	--	$\frac{2M_C + 0.5\alpha}{\sqrt{3}\alpha}$

The choices made for f_d^f and f_p^f and their physical meanings can be described as follows. The form of f_d^f is given by a general Mises type criterion:

$$f_d^f = \frac{3}{2} (S_{ij} - \alpha_{ij}) (S_{ij} - \alpha_{ij}) - k^2 = 0 \quad (19)$$

where $S_{ij} = \sigma_{ij} - \frac{1}{3} \alpha_{kk} \delta_{ij}$

and $\delta_{ij} = 1$ for $i = j$, $\delta_{ij} = 0$ for $i \neq j$

where δ_{ij} is the Kronecker delta, σ_{ij} the stress tensor, S_{ij} the deviatoric stress tensor, and α_{ij} represents the anisotropic state of the material at failure, with k and α_{ij} dependent on the initial state of the material only. If the clay is initially cross-anisotropic (e.g., natural 1-D consolidated clays) the axes of stresses and strains are chosen to coincide with the axes of anisotropy (Fig. 6). If a different coordinate system is chosen, the appropriate direction cosines must be used. For cross-anisotropic clays, $\alpha_{33} = \alpha_{22} = -\alpha_{11}/2$, and $\alpha_{ij} = 0$ for $i \neq j$.

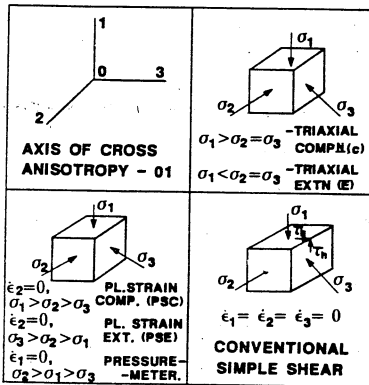


Fig. 6.- Axis System for Different Tests

The form for f_p^f is given by an extended von Mises type criterion:

$$f_p^f = (\sigma_1 - \sigma_2)^2 + (\sigma_2 - \sigma_3)^2 + (\sigma_3 - \sigma_1)^2 - \frac{2H^2}{9} (\sigma_1 + \sigma_2 + \sigma_3)^2 = 0 \quad (20)$$

where σ_1 , σ_2 , and σ_3 are the principal effective stresses and H is a constant. The failure criteria given in Eqs. 19 and 20 are interpretable within the context of mechanics. The terms α_{ij} can be considered to represent the deviatoric component of residual stresses in the clay, that is locked-in stresses indicative of the anisotropic nature of the soil. The deviatoric stresses internally available in the soil are given by $(S_{ij} - \alpha_{ij})$. From an energy standpoint, Eq. 19 can be interpreted in terms of the shear strain energy internally stored in the soil, while Eq. 20 shows that the strain energy externally available to do work is dependent on the mean stress. Taken together, those equations imply that the mean and deviatoric stresses at failure are dependent on the orientation of the failure plane.

The general 3-D failure criteria, Eqs. 19 and 20, should satisfy the conditions $q_f = M p_f$ in TC and TE, and the results obtained using the axisymmetric model given earlier. These conditions can be used to solve for the model parameters α_{ij} , k, and H. The first condition implies that $H^2 = M^2$, and it yields the following relationship between ϕ_c and ϕ_e :

$$\sin\phi_e = \frac{\sin\phi_c}{1 - \frac{2}{3} \sin\phi_c} \quad (21)$$

The predictions made with Eq. 21 are given in Fig. 5 (dashed line) for the experimental data used earlier. The agreement between predicted and experimental values is very good. For comparison, the predictions made using the work by Lade and Mussante (1978), and Matsuoka and Nakai (1982) are also given in Fig. 5. For a given ϕ_c , these relationships tend to underpredict the value of ϕ_e . The results in Fig. 5 indicate that, based upon the TC and TE failure modes, the proposed criteria are satisfactory. However, alternate forms could be explored based upon data for other modes of failure.

Using the second condition that the failure criteria must satisfy, i.e., the axisymmetric results in TC and TE, the two parameters α_{ij} and k in Eqs. 19 and 20 can be solved for:

$$\frac{k}{\sigma_{vo}} = \frac{2M_c + 0.5\alpha}{M_c + \alpha} \left(\frac{\tau_f}{\sigma_{vo}} \right)_{TC} \quad (22)$$

and

$$\frac{\alpha_{11}}{\sigma_{vo}} = \frac{\alpha}{M_c + \alpha} \left(\frac{\tau_f}{\sigma_{vo}} \right)_{TC} \quad (23)$$

where $(\tau_f / \sigma_{vo})_{TC}$ is given by Eqs. 11 or 13.

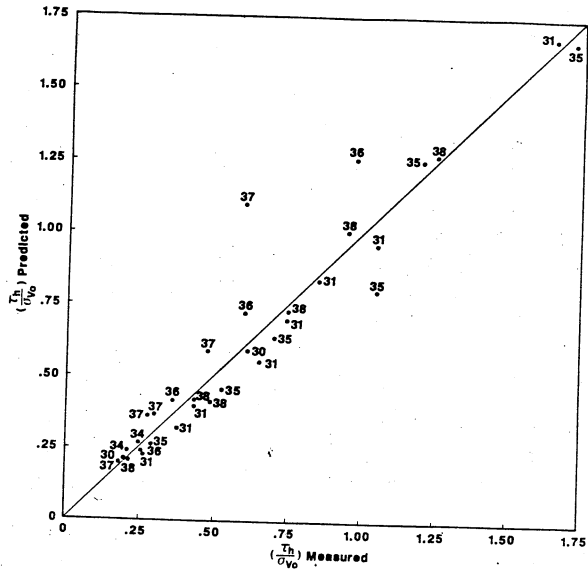


Fig. 7a. Predicted versus Experimental Undrained Strength ratio $(\frac{\tau_h}{\sigma_{vo}})_{SS}$ for many Clays for Different Test

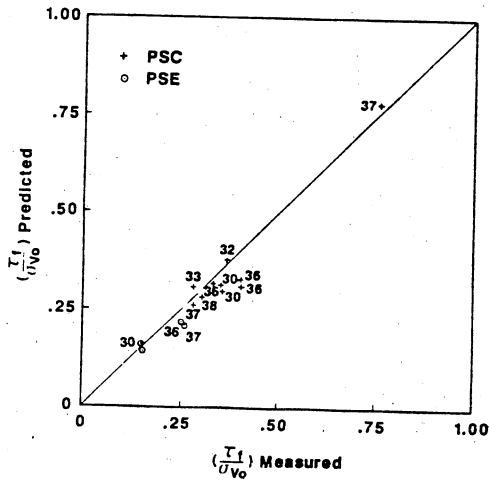


Fig. 7b. Predicted versus Experimental Undrained Strength ratio $(\frac{\tau_f}{\sigma_{vo}})$ in PSC/PSE for many Clays (Numbers refer to Cases in Table 1)

Applications of the Model

Using Eqs. 11 and 17-23, the strength relationships for TC, TE and some of the most commonly encountered modes of failure, as well as additional information on stresses, friction angles, and shear induced pore pressure parameters at failure were developed (see Table 2). Similar information could be derived for any other mode of failure that is of interest. The undrained shear strength relationships for some of the most commonly encountered modes of failure shown in Figure 6 are given by (Thevanayagam 1988):

$$\left(\frac{\tau_f}{\sigma_{vo}}\right)_{SS} = \frac{1.5\alpha}{M_c + \alpha} \left(\frac{\tau_f}{\sigma_{vo}}\right)_{TC} \quad (24a)$$

$$\left(\frac{\tau_{h,SS}}{\sigma_{vo}}\right) = 0.9 \left[\frac{2M_c + 0.5\alpha}{\sqrt{3}(M_c + \alpha)} \right] \left(\frac{\tau_f}{\sigma_{vo}}\right)_{TC} \quad (24b)$$

$$\left(\frac{\tau_f}{\sigma_{vo}}\right)_{PSC} = \frac{\frac{2\sqrt{3}}{3} M_c + 1.04\alpha}{M_c + \alpha} \left(\frac{\tau_f}{\sigma_{vo}}\right)_{TC} \quad (25)$$

$$\left(\frac{\tau_f}{\sigma_{vo}}\right)_{PSE} = \frac{\frac{2\sqrt{3}}{3} M_c + 0.46\alpha}{M_c + \alpha} \left(\frac{\tau_f}{\sigma_{vo}}\right)_{TC} \quad (26)$$

where $\alpha = \gamma \alpha_o$ and $(\tau_f / \sigma_{vo})_{TC}$ is given by Eq. 11 or 13. The factor 0.9 in Eq. 24b was added to the theoretical results to take into account the non-uniformity in the stress distribution in simple shear (SS) tests conducted in laboratory, which was found to reduce the true strength of the clay by about 10% (Prevost and Hoegt 1976). Recalling Eq. 13, 18 and any of the above Eqs. 24-26, it is clear that the following holds true for any particular type of undrained shear in TC/TE, PSC/PSE, and SS:

$$\left(\frac{\tau_f}{\sigma_{vo}}\right)_{OC} = \left(\frac{\tau_f}{\sigma_{vo}}\right)_{nc} \left[OCR\right]^\Delta \quad (27)$$

The Eqs.16,24-27 allows one to relate the triaxial compressive strength to shear strength for many other commonly encountered modes of failure.

Using the Eqs. 17-21, the "b" parameter ($b = (\sigma_2 - \sigma_3) / (\sigma_1 - \sigma_3)$) in PSC at failure is given by:

$$b = \frac{1}{2} \left[\frac{\frac{2.31 M_c}{\alpha} + 0.58}{\frac{2.30 M_c}{\alpha} + 2.08} \right] < \frac{1}{2} \quad (28)$$

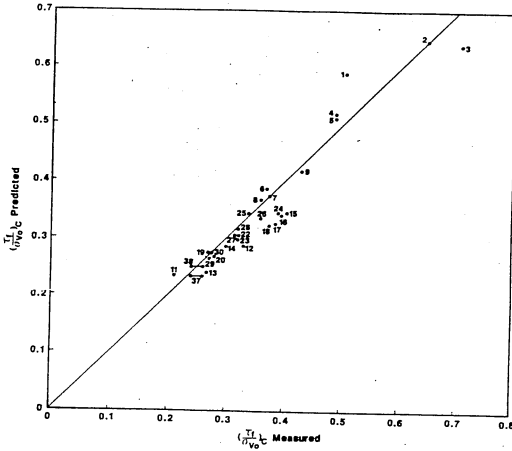


Fig. 8. Predicted versus Experimental Undrained Strength ratio $(\frac{T_f}{\sigma_{vo}})_c$ for many Clays (Numbers refer to Cases in Table 1)

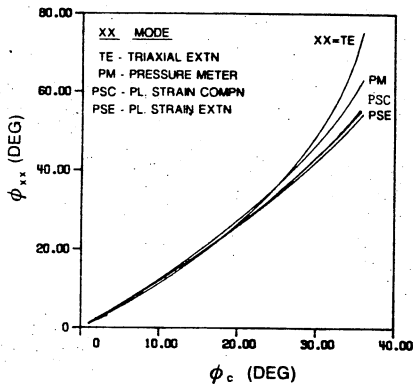
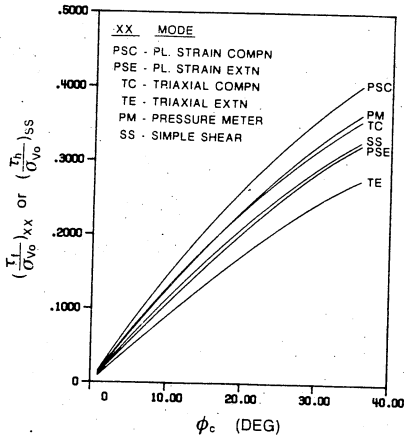


Fig. 9. Simplified Relationship for Undrained Strength Ratio $(\frac{T_f}{\sigma_{vo}})$ for N.C. Clays

Fig. 10. Simplified Relationship Between Friction Angles in Many Modes of Deformation

For isotropic clays, Eq. 28 reduces to $b=1/2$.

For typical soil parameters, the above relationship reduces to: $0.4 < b < 0.5$ which is in the expected range for clays reported by Randolph and Worth (1981). Figs. 7a-b and 8 show the measured and predicted strength of many natural clays, for many different stress paths, geologic origins, and OCR. The close agreement observed in these figures give some confidence to the proposed theory. Invoking Jaky's relationship (1948) for $K_0 (= 1 - \sin \phi_c)$, the relationships for friction angle and undrained shear strength in various modes of failure can be further simplified. Figs. 9 and 10 show these simplified relationships.

Available data collected from the literature indicate that the angle of friction obtained from a isotropic consolidated triaxial test (CIUC) and that from the K_0 consolidated triaxial compression test (CK_0UC) are approximately same (Mayne, 1985). Hence, friction angle from a CIUC test may be a satisfactory input parameter for the proposed model. Thus the data obtained from a simple and inexpensive CIUC test could be used in conjunction with the proposed model to obtain shear strength parameters of 1-D consolidated natural clays.

The general concept of the approach and the advantages of this method may be summarized by: (i) the notion that mean stress at failure is dependent on mode of undrained failure is included; (ii) One axisymmetric yield surface and a general form for the failure surface f^f are introduced, which allow the complete determination of failure parameters independently; (iii) The initial anisotropy is appropriately modelled through the parameters α_{ij} and α_0 and the effect of induced anisotropy is introduced through γ . Given the initial conditions of the soil, the complete failure behavior at critical state (strength, pore pressure, friction angle, etc.) along any mode of failure is given by the relationships presented in Table 2; (iv) Little laboratory testing of soil is required to calibrate the model; (v) Any relationship derived in this work can be related using ϕ_c and OCR (with $k_v/\lambda = 0.2$ and (vi) The model is kept very simple and versatile for field use using a hand calculator.

Conclusion

Based on recent developments in Cam Clay models and a 3-D failure criterion, an anisotropic model has been developed to study the behavior of clays at critical state. The model is simple, and holds the promise of being very successful, as shown by comparisons with available data. With these developed relationships one can predict the strength (and other failure parameters), in any particular mode of failure. In addition, given the failure conditions in any one mode of deformation, one can transform the data to predict the behavior in a different mode of deformation. This is possible

but with little additional testing. It is also possible to transform the test data obtained from a simple and inexpensive CIUC test to obtain shear strength parameters of 1-D consolidated natural clays. This increased capability appears to have the potential to markedly improve the geotechnical engineer's capability in design analysis.

Acknowledgments

The writer is thankful to Prof. A. Thurairajah, pioneer of cam-clay models, for his encouragement and the reviewers of the Sri Lankan Geotechnical Engineering Society for their constructive criticism of this paper.

Appendix I - References

1. Atkinson, J.II., Richardson, D., and Robinson, P.J. (1987) "Compression and Extension of K_0 Normally Consolidated Kaolin Clay", J. Geotech. Engg. Div., ASCE, 113(12).
2. Brooker, E. W. and Ireland, H. O., (1965) Earth Pressure at Rest Related to Stress History", Can. Geotech. Journal, Vol. 2, No 2, pp. 1-15.
3. Dafalias, Y. F. and Herrman L. R. (1982), "A Generalized Bounding Surface Constitutive Model for Clays", chapter in Application of Plasticity and Generalized Stress-Strain in Geotechnical Engineering, pp. 78-95, R. N. Young and E. T. Selig, eds., Special Publication Series by ASCE.
4. Dafalias, Y. F. (1987), "An Anisotropic Critical State Clay Plasticity Model", Constitutive Laws for Engineering Materials Theory and Applications, Vol. 1 (C.S. Desai, et. al., eds.), pp. 513-522.
5. D'Appolonia, D. J., Lambe, T.W., and Poulos, H.G. (1971), "Evaluation of Pore Pressure Beneath an Embankment", Journal of Soil Mechanics and Foundation Division, ASCE, Vol. 97, SM6, pp. 881-897.
6. Dickey, J. W., Ladd, C. C., and Rixner, J. J. (1968), "A Plane Strain Shear Device for Testing Clays, " Research Report R68-3, Soils Publication No 237, Department of Civil Engineering, MIT, January.
7. Duncan, I. M. and Seed, H. B. (1966) "Anisotropy and Stress Reorientation in Clay, " ASCE J. Soil Mech. Found. Engg. Div., (92), No. 5, 21-50.
8. Jaky, J. (1948), "Pressures in Silos", Proceedings of the Second International Conference in Soil Mechanics and Foundation Engineering, Rotterdam, Netherlands, Vol. 1, pp. 103-107.
9. Graham, J., Noonan, M.L., and Lew, K.V. (1983) "Yield States and Stress Strain Relationships in a Natural Plastic Clay", Can. Geotech. J. (20), 502-516.
10. Kavvasdas, M. (1982), "Non Linear Consolidation Around Driven Piles", D.Sc. Thesis, MIT, Cambridge, Massachusetts, 666 pp.

11. Lacasse, S. M. and Ladd, C. C (1973) "Behavior of Embankments on New Liskeard Varved Clay, "Research Report R73-44, Soils Publication No. 327, Department of Civil Engineering, MIT.
12. Ladd, C. C. and Edgers, L. (1972), "Consolidated Undrained Direct-Simple Shear Test on Saturated Clays," Research Report R72-82, MIT.
13. Ladd, C.C. and Foott, R. (1974) " New Design Procedure for Stability of Soft Clays, " J. Geotech. Rngg. Div., ASCE, 100 (GT7), 763-786.
14. Ladd, C. C., Foott, R., Ishihara, K., Schlosser, F., and Poulos, H.G. (1977), "Stress-Deformation and Strength Characteristics", Proc. 10th Int. Conf. Soil Mech. Found. Engrg., Vol. 1, Tokyo, Japan.
15. Lade, P. V. and Musante, AH.M. (1977), "Failure Conditions in Sand and Remoulded Clay", Proc. 9th Int. Conf. Soil Mech. Found. Engrg., Tokyo, Japan, Vol. 1, pp. 181-186.
16. Lade, P. V. and Musante, H.M. (1978), "Three Dimensional Behavior of Remoulded Clay", Geotech. Engrg. Div., ASCE, Vol. 104, GT2, pp. 193-209.
17. Lewin, P.I (1973) "The Influence of Stress History on Plastic Potential," Proceedings Symposium on Role of Plasticity in Soil Mechanics, Cambridge, 96-105.
18. Matsuoka, H. and Nikai, T. (1982), " A New Failure Criterion for Soils in Three Dimensional Stresses", Proceedings IUTAM Symposium, Deformation Failure of Granular Materials, Delft.
19. Mayne, P.W. (1985) "Stress Anisotropy Effects on Clay Strength" ASCE, Journal of Geotechnical Engg. Div., Vol.III, No. 3, pp. 356-366.
20. Mitachi, T, and Kitago, S. (1979), " The Influence of Stress History and Stress System on the Stress-Strain-Strength Properties of Saturated Clay, "Soils and Foundations, Vol. 19, No. 2, pp. 45.
21. Nakase, A. and Kamei, T. (1983), "Undrained Shear Strength Anisotropy of Normally Consolidated Cohesive Soils, "Soils and Foundations, Vol. 23, No. 1, pp. 91-101.
22. Parry, R.H.G. and Nadarajah, V. (1974), "Observations on Laboratory Prepared, Lightly Overconsolidated Specimens of Kaolin, "Geotechnique, Vol. 24, No. 3, pp 345-358.
23. Prevost, J.H. (1979), "Undrained Shear Tests on Clays", Journal of the Geotechnical Engineering Division, ASCE, Vol. 105, GT1, pp. 49-64.
24. Prevost, J. H. and Hoeg, K., (1976) "Reanalysis of Simple Shear Soil Testing", Can. Geotech, J. (13), 418-429.
25. Randolph, M.F. and Wroth, C. P. (1981) "Application of the Failure State in Undrained Simple Shear to the Shaft Capacity of Driven Piles, "Geotechnique (31), 143-157.
26. Roscoe, K. H. Schofield, A. N., and Thurairajah, A. (1963), "On Yielding of Clays in States Wetter than Critical", Geotechnique, Vol. 13, No. 3, pp. 211-240.
27. Roscoe, K.H. and Burland, J. B. (1968), "On the Generalized Stress-Strain behavior of Wet Clay", Engineering Plasticity, (J. Heyman and F.A.

- Leckie, eds.), pp. 535-609, Cambridge University Press.
28. Saada, A.S. and Bianchini, G. F. (1975), "Strength of One Dimensionally Consolidated Clays", Journal of the Geotech, Engrg. Div., ASCE, Vol. 101, GT11, pp. 1151-1164.
 29. Schofield, A.N. and Wroth, C. P. (1968), "Critical State Soil Mechanics", McGraw-Hill Book Co., London, England, 310 pp.
 30. Sivakugn, N. (1987), "Effects of Stress Path and Anisotropy on the Interpretation of the Pressuremeter Test Results", Ph.D. Thesis, Purdue University, 204 pp.
 31. Tavenas, F. and Leroueil, S. (1977) "Effects of Stresses and Time on Yielding of Clays", "Proc. 9th Int. Conf. Soil Mech. Found. Engrg., Tokyo, Japan.
 32. Thevanayagam, S., Skandarajah, A., and Chameau, J.L. (1988), "Anisotropy and Stress path Effects in Clays with Applications to the Pressuremeter Test", Airforce Office of Scientific Research, Bolling AFB, D.C., 135 p.
 33. Thevanayagam, S. (1988), "A simple Anisotropic Model for Critical State behavior of Clays", Internal Report, CE-GEOT-88-1, Purdue University, W. Lafayette, IN., 57 p.
 34. Tevanayagam, S. and Prapaharan, S. (1989), "Compression and Extension of KConsolidated Kaolin Clay", Discussion, Journal of Geot. Engrg. Div., ASCE, Vol. 115, No. 8.
 35. Ting (1968) "Some Effects of History of the Stress-Strain Behavior of Kaolin," Ph.D. Thesis, University of Cambridge, England.
 36. Wroth, C. P. (1984), "The Interpretation of In Situ Soil Tests", Rankine Lecture, geotechnique, Vol. 34, No. 4, pp. 449-489.

Appendix II - Notation

- A_f - Skempton's A-parameter at failure;
 CIUC - isotropically consolidated undrained triaxial compression test;
 CK_{OUC} - 1-D consolidated undrained triaxial compression test;
 CSL - critical state line;
 e - void ratio;
 f - $f(p, q, r_n)$ - yield surface
 f^f - failure criterion;
 G - shear modulus;
 K - bulk modulus;
 K_o - coefficient of earth pressure at rest;
 K_{oNCL} - 1-D consolidated normal compression line in e vs $\ln(p)$ plane;
 M - q/p , stress ratio at critical state;
 N_o - specific volume intercept of the normal compression line in v vs. $\ln(p)$ at $p=1$ kPa.
 PSC - plane strain compression;

- PSE - plane strain extnsion;
 SS - simple shear;
 TC - triaxial compression;
 TE - triaxial extension;
 p - mean effective stress, $(\sigma_1 + \sigma_2 + \sigma_3)/3$;
 p_e - $\exp(N_o - v/\lambda)$, equivalent pressure;
 q - deviatoric effective stress $(\sigma_1 - \sigma_3)$;
 r_n - memory variable, hardening parameter;
 v - $1+e$, specific volume;
 v^λ - $(v + \lambda \ln(p))$, equivalent specific volume;
 Γ^λ - specific volume intercept of the critical state line in v vs. $\ln(p)$ plane at $p=1$ kPa;
 α - anisotropic parameter;
 α_o - anisotropic parameter at virgin consolidated state;
 α_{ij} - anisotropic tensor;
 ϵ_{ij} - strain tensor;
 ϵ_v - $(\epsilon_1 + 2\epsilon_3)$ volumetric strain;
 ϵ_v^q - $2/3(\epsilon_1 - \epsilon_3)$ deviatoric strain;
 k, k_v - slope of the swelling lines in $e-\ln(p)$ plane and in $e-\ln(\sigma_v)$ plane; respectively;
 λ, λ_v - slope of the normal compression and critical state lines in $e-\ln(p)$ and $e-\ln(\sigma_v)$ plane, respectively; $v =$ Poisson's ratio;
 η - q/p , stress ratio;
 η_o - $(q/p)_o$, stress ratio during virgin consolidation;
 ϕ - effective angle of shearing resistance;
 σ - stress tensor;
 τ_h - peak shear strength, $(\sigma_1 - \sigma_3)/2$ at failure;
 τ_h - peak horizontal shear stress at failure in simple shear;
 $\Delta \tau_{sh}$ - shear induced pore pressure;

Subscripts:

- c - with respect to triaxial compression;
 e - with respect to triaxial extension;
 nc - normally consolidated clay;
 oc - overconsolidated clay;
 vo - initial state in vertical direction

Superscripts:

- e - elastic part
 p - plastic part
 . - increment

GUIDE FOR AUTHORS

Manuscripts of original papers, technical notes, and discussions should be submitted to the Editor, Sri Lankan Geotechnical Journal, SLGS Secretariat, c/o National Building Organisation, 99/1, Jawatta Road, Colombo 05, Sri Lanka.

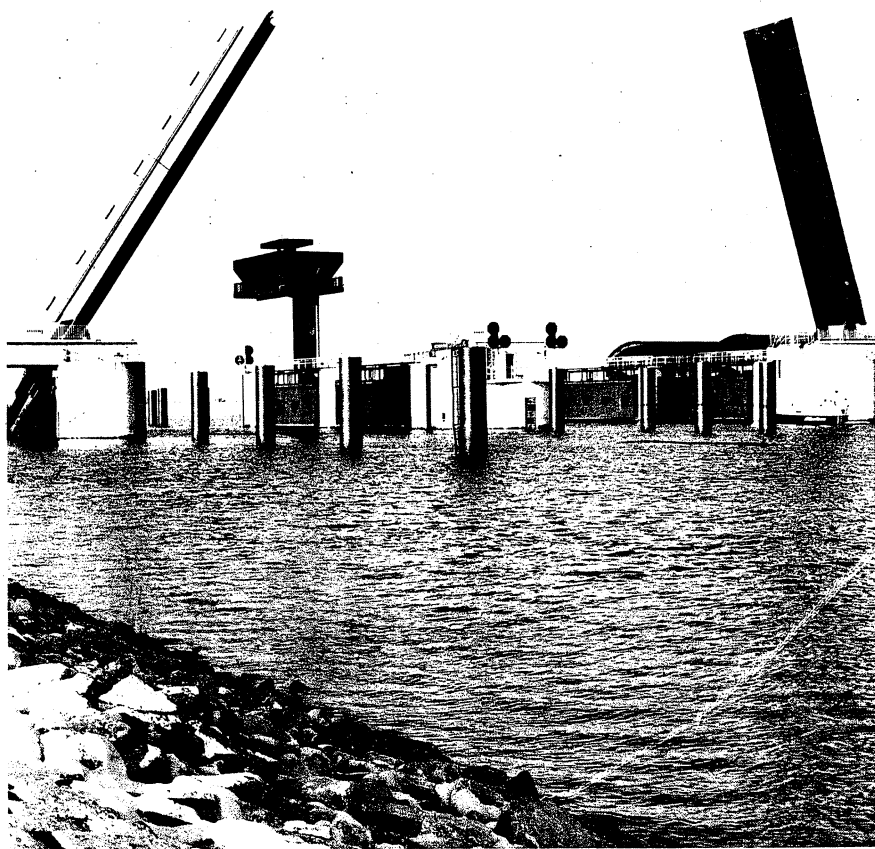
The following notes will serve as a guide for authors.

1. Authors need not be members of the Sri Lankan Geotechnical Society.
2. The manuscript should be typed double-spaced on one side of A4.
3. The full name of the author (s), present employment (s), and an abstract of not more than 200 words must appear on the first page of the paper.
4. The length of a paper should be within 10,000 word - equivalents. Each full manuscript page may be approximated to 300 words (i.e. average of 72 characters per line and 25 lines per page).
5. Figures should be clearly drawn in black ink on one side of good quality paper (preferably tracing paper). Illustrations should not be more than twice the size of the final production which will be a maximum width of 110mm. The lettering must be legible at the reduced size. Photographs should be submitted as black and white glossy print. No captions should be placed on illustrations but they should be listed on a separate sheet. All illustrations should be numbered consecutively in Arabic numbers.
6. Tables should be numbered consecutively with Arabic numbers. They should be typed on separate sheets at the end of the manuscript.
7. Symbols should be defined when they first appear and should conform as far as possible with the list given in the ISSMFE Lexicon (1981) (This is available at the SLGS Secretariat for references). All symbols should be alphabetically arranged in an appendix.
8. SI units should be adopted throughout the paper as a rule. If any other units are used, they must be accompanied by the SI units in parentheses.
9. Referenced should appear in the text within parentheses, with the Authors' name in capitals followed by the year of publication. A list of references should appear immediately following the text in alphabetical order of Authors' names. No abbreviation should be used other than those for volume, number and page.
10. Proofs will be sent to the first author only, for correction of printing errors and returned within a week. No new material should be inserted in the text at the time of proof reading.
11. The Manuscript should not have been previously published nor should it be under consideration for publication elsewhere.

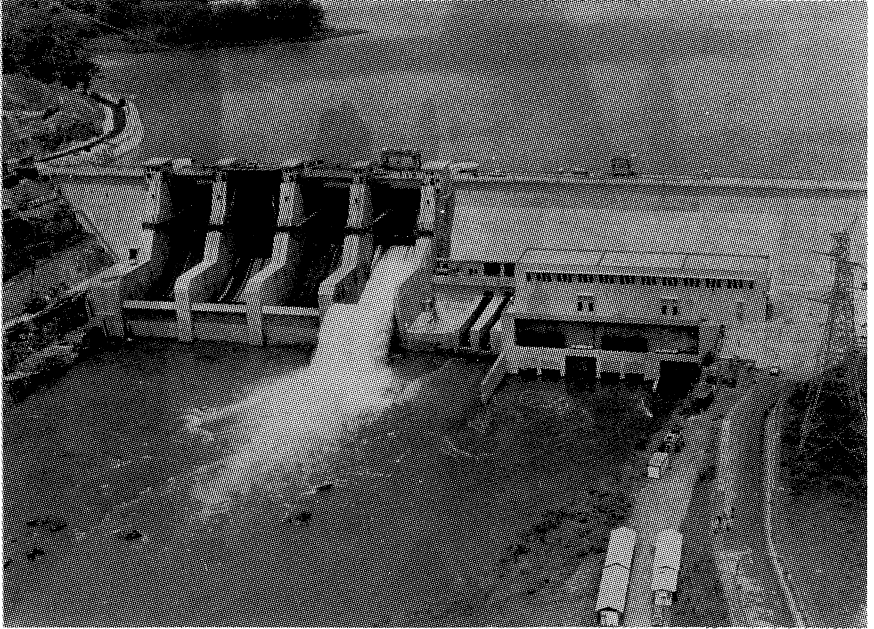
DSD
DILLINGER STAHLBAU GMBH
P.O. Box 1340
Henry - Ford - Strasse
D 6630 Saarlouis, W - Germany.
Tel: (06831) 181
Telex: 443724

**Hydraulic
Steel
Structures**

DSD



ZHR  



With the Compliments from

JOINT VENTURE ZÜBLIN-HOCHTIEF
CIVIL CONTRACTORS FOR THE
RANTEMBE HYDROPOWER PROJECT

GEOTECHNICAL ENGINEERING SERVICES

Our laboratories are well-equipped with modern equipment to cater for research and consultancy needs. Our services include:

- * Extensive range of field and laboratory tests and comprehensive investigation reports.
- * Special consultancy services for construction particularly on weak sub-soils, expansive soils and residual soils.
- * Expertise in special foundation techniques including ground improvement, under-pinning, micro piling, under-reamed piling.
- * Quality control in land reclamation and development.
- * Landslide investigations and slope stabilisation.
- * Geotechnical mapping and landslide hazard mapping.
- * Expertise in restoration of distressed foundations and buildings.
- * Boring in all soils and in rocks and field tests - including static and dynamic penetration tests, CBR and plate load bearing tests, vane shear tests etc.,
- * Laboratory testing for physical, chemical and mechanical characteristics of soils and rocks.



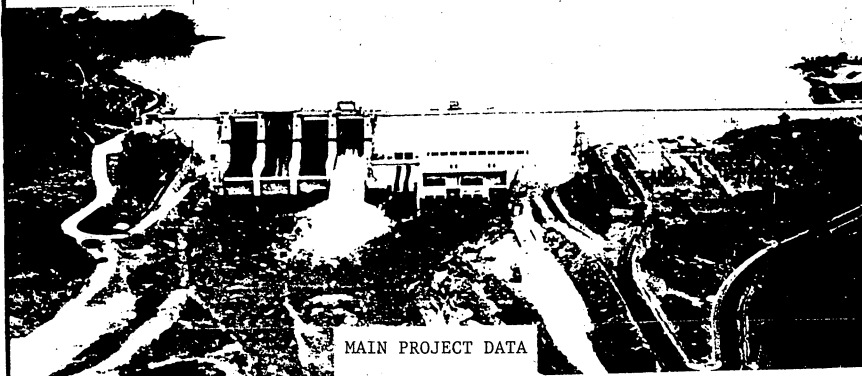
MINISTRY OF POLICY PLANNING AND IMPLEMENTATION

NATIONAL BUILDING RESEARCH ORGANISATION

99/1, JAWATTA ROAD. COLOMBO - 5. SRI LANKA. TELEPHONE: 588946

RANTEMBE MULTIPURPOSE DAM

Last of the Mahaweli Dams



MAIN PROJECT DATA

RESERVOIR

Active Storage 9.7 MCM

DAM

Concrete Gravity type
Height 41.5 m
Volume 200,000 m³
Length 420 m

SPILLWAY

Capacity 10,235 m³/s
Gates 4 Tainter
Gate weight 115 t each

POWER WATERWAYS

Capacity 2 x 90 m³/s
Penstocks 2 of 50 m length
4.3 m dia
Gates 2 service gates(slide)
2 revision gates(stoplogs)

BOTTOM/IRRIGATION OUTLET

Capacity 2 x 150 m³/s
Gates 2 service gates(Tainter)
2 revision gates(Slide)

POWERHOUSE

Turbines 2 x 27.2 MW Francis
Annual energy production approx. 250 GWh total
approx. 180 GWh firm

We proudly announce
the successful completion

CONSULTING ENGINEERS

Joint Venture Randenigala (JVR):

Salzgitter Consult GmbH, Fed. Rep. of Germany
Electrowatt Engineering Services Ltd., Switzerland
Agrar-und Hydrotechnik GmbH, Fed. Rep. of Germany

In cooperation with:

Central Engineering Consultancy Bureau (CECB), Colombo